

# Transformed Diffusion-Wave fPINNs: Enhancing Computing Efficiency for PINNs Solving Time-Fractional Diffusion-Wave Equations

Zhengqi Zhang<sup>a</sup>, Jing Li<sup>a,\*</sup>

<sup>a</sup>Zhejiang Lab, Hangzhou, 311121, China

---

## Abstract

We propose transformed Diffusion-Wave fractional Physics-Informed Neural Networks (tDWfPINNs) for efficiently solving time-fractional diffusion-wave equations with fractional order  $\alpha \in (1, 2)$ . Conventional numerical methods for these equations often compromise the mesh-free advantage of Physics-Informed Neural Networks (PINNs) or impose high computational costs when computing fractional derivatives. The proposed method avoids first-order derivative calculations at quadrature points by introducing an integrand transformation technique, significantly reducing computational costs associated with fractional derivative evaluation while preserving accuracy. We conduct a comprehensive comparative analysis applying this integrand transformation in conjunction with both Monte Carlo integration and Gauss-Jacobi quadrature schemes across various time-fractional PDEs. Our results demonstrate that tDWfPINNs achieve superior computational efficiency without sacrificing accuracy. Furthermore, we incorporate the proposed approach into adaptive sampling approaches such as the residual-based adaptive distribution (RAD) for the time-fractional Burgers equation with order  $\alpha \in (1, 2)$ , which exhibits complex solution dynamics. The experiments show that the Gauss-Jacobi method typically outperforms the Monte Carlo approach; however, careful consideration is required when selecting the number of quadrature points. Overall, the proposed tDWfPINNs offer a significant advancement in the numerical solution of time-fractional diffusion-wave equations, providing an accurate and scalable mesh-free alternative for challenging fractional models.

**Keywords:** Physics Informed Neural Networks, Time-fractional Partial Differential Equations, Diffusion-wave

---

## 1. INTRODUCTION

In recent years, fractional and nonlocal models have attracted considerable interest owing to their broad applications in diverse disciplines, including physics, engineering, biology, and finance. Time-fractional diffusion-wave partial differential equations (PDEs) (1), in particular, have been extensively used to model the propagation of mechanical waves in viscoelastic media [1, 2]. Furthermore, such equations are instrumental in modeling the fractional dynamics of systems relevant to medicine [3, 4]. For a comprehensive overview of the applications of fractional models in biology and physics, readers are referred to [5, 6].

Nevertheless, solving time-fractional partial differential equations (TFPDEs) of diffusion-wave type presents significant challenges, primarily stemming from their inherent nonlocality and wave-like characteristics. Analytical solutions involving Mittag-Leffler and Wright functions have been introduced in [7, 8, 9]. To overcome these difficulties, a variety of numerical methods have been developed, including finite-difference methods [10, 11], convolution-quadrature methods [12, 13], collocation-type methods [14, 15], and spectral methods [16, 17].

In recent years, the rapid advancement of computing resources and machine learning methodologies has brought Physics-Informed Neural Networks (PINNs) [18, 19, 20] to the forefront of scientific computing. PINNs have attracted considerable attention due to their efficacy in solving partial differential equations (PDEs), particularly benefiting from their mesh-free formulation, which alleviates the curse of dimensionality. To address the computational challenges

---

\*Corresponding author

Email addresses: zhengqizhang@zhejianglab.org (Zhengqi Zhang), lijing@zhejianglab.org (Jing Li)

associated with incorporating fractional derivatives into the PINNs framework, various numerical approximation techniques have been proposed. Among these, the fractional Physics-Informed Neural Networks (fPINNs), as proposed in [21], have been widely adopted. The core strategy of fPINNs involves applying automatic differentiation for integer-order operators, while approximating fractional derivatives using numerical discretization schemes-typically based on finite difference-applied to the neural network outputs. For further developments in this direction, readers are referred to [22, 23].

Despite their practical utility, these finite-difference-based schemes for fractional derivatives inherently rely on discretization grids, thereby compromising the mesh-free advantages that distinguish PINNs. Recent theoretical investigations [24, 25] have shown that PINNs exhibit a hierarchical spectral bias: they preferentially learn the low-frequency components of the solution, while accurate resolution of high-frequency features is delayed. This spectral bias imposes significant challenges in accurately capturing multiscale dynamics and motivates the development of advanced training strategies, such as adaptive sampling methods [26, 27]. Building upon these advances, the present study proposes a fully mesh-free computational framework for the treatment of fractional derivatives, preserving the core advantages of PINN-based approaches.

Spectral methods [28, 29] have been proposed to reformulate problems involving fractional derivatives by transforming the original time-space domain into the frequency domain. Although this approach effectively avoids direct numerical evaluation of fractional operators, it typically incurs elevated computational costs and may suffer from reduced accuracy due to the inverse transform. Alternatively, Monte Carlo fractional Physics-Informed Neural Networks (MCfPINNs) [30] leverage stochastic sampling to approximate both temporal and spatial fractional derivatives. Building on this framework, recent studies [31, 32] have introduced Gauss-Jacobi quadrature rules to improve computational efficiency by replacing Monte Carlo integration with stochastic quadrature rules. Notably, both the Monte Carlo and the Gauss-Jacobi quadrature approaches can be seamlessly integrated into adaptive sampling frameworks, preserving the mesh-free character of PINN-based approaches and making them particularly well-suited for applications in fractional-order modeling within machine learning frameworks.

In this work, we consider an initial-boundary value problem of diffusion wave equation with order  $\alpha \in (1, 2)$ :

$$\begin{aligned} \partial_t^\alpha u(t, \mathbf{x}) + \mathcal{N}(u(t, \mathbf{x}), f(t, \mathbf{x})) &= 0, \quad (t, \mathbf{x}) \in (0, T] \times \Omega, \\ u(t, \mathbf{x}) &= 0, \quad (t, \mathbf{x}) \in (0, T] \times \partial\Omega \\ u(0, \mathbf{x}) &= a(\mathbf{x}), \partial_t u(0, \mathbf{x}) = b(\mathbf{x}), \quad \mathbf{x} \in \Omega, \end{aligned} \quad (1)$$

where  $T > 0$  denotes the final time,  $\Omega \subset \mathbb{R}^d$  ( $d = 1, 2, 3$ ) is a convex polyhedral domain with boundary  $\partial\Omega$ .  $\mathcal{N}$  is a time-independent differential operator acting on the solution  $u$  and the source term  $f$ .  $\partial_t^\alpha u$  denotes the Caputo fractional derivative of order  $\alpha \in (1, 2)$  with respect to time  $t$ , defined as [33, P. 70],

$$\partial_t^\alpha u(t) = \frac{1}{\Gamma(2-\alpha)} \int_0^t (t-\tau)^{1-\alpha} \frac{d^2}{d\tau^2} u(\tau) d\tau, \quad (2)$$

where  $\Gamma$  denote the Gamma function.

In recent years, various PINNs-based methods have been proposed to address diffusion-wave problems. For example, [23] employed fPINNs to solve time-dependent diffusion-wave equations, while Lu et al. [22] utilized the  $L2$  scheme to approximate Caputo fractional derivatives for  $\alpha \in (0, 2)$ . Chen et al. [29] applied the Laplace transform to reformulate the problem described by (1), and Lin et al. [32] integrated tensor neural networks with Gauss-Jacobi quadrature to achieve high-accuracy estimation. Nevertheless, there remains a significant gap in the development of mesh-free methods for computing fractional derivatives of order  $\alpha \in (1, 2)$ . A commonly adopted approach is to extend the MCfPINNs framework-originally proposed for  $\alpha \in (0, 1)$ -using either the Monte Carlo (MC) method [30] or Gauss-Jacobi (GJ) quadrature [31]. However, both approaches, as well as the methodology in [32] face practical challenges when interfaced with the automatic differentiation capabilities of mainstream machine learning frameworks such as PyTorch and TensorFlow. In particular, computing derivatives at quadrature points often incurs considerable computational overhead.

To address the aforementioned challenges, we propose transformed Diffusion-Wave fractional Physics-Informed Neural Networks (tDWfPINNs), an efficient and fully mesh-free computational framework for handling fractional derivatives of  $\alpha \in (1, 2)$  within the MCfPINNs paradigm. We develop a novel numerical integration scheme which,

in contrast to existing Monte Carlo and Gauss-Jacobi quadrature-based methods [32, 31, 30], avoids differentiation at quadrature points. This modification significantly reduces computational overhead and enhances compatibility with advanced training strategies. Furthermore, the proposed method is seamlessly integrated with adaptive sampling approaches such as the RAD framework, thereby enabling more efficient solutions for a broad class of time-fractional partial differential equations (TFPDEs).

We summarize the main contributions of this paper as follows:

- **A novel computational method for Caputo time-fractional derivatives of order  $\alpha \in (1, 2)$ :** We propose a computational strategy of integrand transformation for time-fractional derivatives of order  $\alpha \in (1, 2)$  that enhances the efficiency of MCfPINNs. Unlike direct approaches, the proposed transformed approach eliminates the need for differentiation at quadrature points, thereby streamlining the computational process and yielding significant savings in computational resources.
- **Comprehensive study on a suite of TFPDEs:** We conduct an in-depth study on the Monte Carlo and Gauss-Jacobi quadrature approaches across a diverse set of TFPDEs. The results indicate that the proposed tDWfPINNs achieve significantly improved computational efficiency. The Gauss-Jacobi method demonstrates superior performance in both accuracy and efficiency, though careful consideration is required when selecting the optimal number of quadrature points to balance computational cost and solution fidelity.
- **Integration of adaptive sampling with tDWfPINNs:** Furthermore, we integrate the RAD method [26] into the tDWfPINNs framework to enhance training efficiency and solution accuracy. Through systematic experiments across a range of fractional orders  $\alpha$ , we demonstrate that the integration of RAD improves convergence behavior and facilitates the effective resolution of challenging TFPDEs.

This paper is organized as follows. In Section 2, we introduce the framework of Physics-Informed Neural Networks (PINNs) and review the original numerical approaches based on MCfPINNs. Section 3 presents the proposed tDWfPINNs method for fractional derivatives of order  $\alpha \in (1, 2)$ . In Section 4, we evaluate the performance of the proposed method through a series of numerical experiments on TFPDEs, comparing various integration techniques in terms of computational efficiency and solution accuracy.

## 2. Preliminaries

In this section, we introduce the framework of PINNs related to the TFPDE (1) and the original numerical approaches based on the MCfPINNs.

We begin by considering the abstract formulation of the diffusion-wave equation in Eq. (1). Given the initial conditions  $a$  and  $b$ , the source term  $f$ , and a time-independent differential operator  $\mathcal{N}$ , our objective is to approximate the solution  $u(t, x)$  in  $(0, T] \times \Omega$ .

### 2.1. Physics-Informed Neural Networks (PINNs)

We briefly review the PINNs framework for solving Eq. (1), based on the formulation introduced in [18]. Let  $u(t, x; \theta)$  denote a neural network (NN) representation with parameter set  $\theta$  as an approximation to the true solution  $u(t, x)$ . PINNs are trained by minimizing a loss function that enforces agreement with the underlying PDE, initial conditions, and boundary conditions.

**PDE loss:** Let  $\{t_i^{in}, \mathbf{x}_i^{in}\}_{i=1}^{N_{in}} \subset (0, T] \times \Omega$  be a set of collocation points in the domain. The PDE loss is defined as

$$\mathcal{L}_{in}(\theta) = \frac{1}{N_{in}} \sum_{i=1}^{N_{in}} \left| \bar{\partial}_\tau^\alpha u(t_i^{in}, \mathbf{x}_i^{in}; \theta) - \mathcal{N}(u(t_i^{in}, \mathbf{x}_i^{in}; \theta), f(t_i^{in}, \mathbf{x}_i^{in})) \right|^2 \quad (3)$$

where  $\bar{\partial}_\tau^\alpha u(t_i^{in}, \mathbf{x}_i^{in}; \theta)$  denotes a numerical approximation of the Caputo fractional derivative  $\partial_\tau^\alpha u(t_i^{in}, \mathbf{x}_i^{in}; \theta)$ .

**Boundary Loss:** Let  $\{t_i^{bd}, \mathbf{x}_i^{bd}\}_{i=1}^{N_{bd}} \subset (0, T] \times \partial\Omega$  be a set of boundary points. The boundary loss is given by

$$\mathcal{L}_{bd}(\theta) = \frac{1}{N_{bd}} \sum_{i=1}^{N_{bd}} \left| u(t_i^{bd}, \mathbf{x}_i^{bd}; \theta) \right|^2. \quad (4)$$

**Initial Loss:** Let  $\{\mathbf{x}_i^{init}\}_{i=1}^{N_{init}}$  at  $t = 0$  be a set points at the initial time  $t = 0$ . The loss for enforcing initial conditions is defined as

$$\mathcal{L}_{init}(\theta) = \frac{1}{N_{init}} \sum_{i=1}^{N_{init}} \left| u(0, \mathbf{x}_i^{init}; \theta) - a(\mathbf{x}_i^{init}) \right|^2 + \frac{1}{N_{init}} \sum_{i=1}^{N_{init}} \left| \partial_t u(0, \mathbf{x}_i^{init}; \theta) - b(\mathbf{x}_i^{init}) \right|^2. \quad (5)$$

Together, these components define the composite loss function used to train the neural network approximation in the PINNs framework. **Time-fractional diffusion-wave Problem:**  $\theta$  is obtained by minimizing the following loss function:

$$\theta = \arg \min_{\theta \in \Theta} \mathcal{L}_F(\theta) = \arg \min_{\theta \in \Theta} \mathcal{L}_{in}(\theta) + \lambda_{bd} \mathcal{L}_{bd}(\theta) + \lambda_{init} \mathcal{L}_{init}(\theta), \quad (6)$$

where the weights  $\lambda_{in}$ ,  $\lambda_{bd}$  and  $\lambda_{init}$  is specified before training.

## 2.2. Improved MCfPINN for $\alpha \in (0, 1)$

PINNs have demonstrated significant promise in solving a wide range of PDEs with integer- order derivatives, largely due to the availability of automatic differentiation tools in modern machine learning frameworks such as TensorFlow, PyTorch, and JAX. Their ease of implementation and reliable approximation capabilities have contributed to their growing popularity in scientific computing. However, encoding fractional derivatives directly in PINNs is nontrivial. A fundamental challenge arises from the failure of the classical chain rule in the context of fractional calculus, which impedes the use of automatic differentiation for computing fractional-order derivatives. To address this, a numerical approach based on the substitute form of fractional derivatives for  $\alpha \in (0, 1)$  has been introduced in [30, 31], fully exploiting the tensor-paralleled and mesh-free properties of PINNs.

Firstly, we introduce a lemma that provides an alternative representation of the Caputo fractional derivative. A detailed proof can be found in [34, Lemma 2.10]:

**Lemma 2.1.** *Let  $\alpha \in (n - 1, n)$ ,  $n \in \mathbb{N}$ . Given a sufficiently smooth function  $f$ , we have*

$$\begin{aligned} \partial_t^\alpha f(t) &= \frac{f^{(n-1)}(t) - f^{(n-1)}(0)}{\Gamma(n - \alpha)t^{\alpha-n+1}} + \frac{\alpha - n + 1}{\Gamma(n - \alpha)} \int_0^t \frac{f^{(n-1)}(t) - f^{(n-1)}(\tau)}{(t - \tau)^{\alpha-n+2}} d\tau \\ &= \frac{f^{(n-1)}(t) - f^{(n-1)}(0)}{\Gamma(n - \alpha)t^{\alpha-n+1}} + \frac{\alpha - n + 1}{\Gamma(n - \alpha)} t^{n-\alpha} \int_0^1 \frac{f^{(n-1)}(t) - f^{(n-1)}(t - t\tau)}{t\tau} \tau^{n-1-\alpha} d\tau, \end{aligned} \quad (7)$$

where  $f^{(k)}(t)$  means the  $k$ -th derivative of  $f$  at  $t$ .

For  $n = 1$ , the transformation degenerates to

$$\begin{aligned} \partial_t^\alpha f(t) &= \frac{f(t) - f(0)}{\Gamma(1 - \alpha)t^\alpha} + \frac{\alpha}{\Gamma(1 - \alpha)} t^{1-\alpha} \int_0^1 \frac{f(t) - f(t - t\tau)}{t\tau} \tau^{-\alpha} d\tau \\ &= \frac{1}{\Gamma(1 - \alpha)} \left\{ \frac{\alpha}{1 - \alpha} t^{1-\alpha} \mathbb{E}_{\tau \sim \text{Beta}(1-\alpha, 1)} \left[ \frac{f(t) - f(t - t\tau)}{t\tau} \right] + \frac{f(t) - f(0)}{t^\alpha} \right\}. \end{aligned} \quad (8)$$

The basic idea of MC-fPINN[30] is to approximate the Caputo fractional derivative  $\partial_t^\alpha f(t)$  using a Monte Carlo approach based on the integral representation in equation (8). To mitigate numeric blow-ups when some samples are very small, the authors set some hyperparameters, i.e., let  $\tau_\varepsilon = \max\{\tau, \varepsilon t^{-1}\}$  given fixed  $\varepsilon_t$ . This yields the approximation:

$$\partial_t^\alpha f(t) \approx \frac{1}{\Gamma(1 - \alpha)} \left\{ \frac{\alpha}{1 - \alpha} t^{1-\alpha} \mathbb{E}_{\tau \sim \text{Beta}(1-\alpha, 1)} \left[ \frac{f(t) - f(t - t\tau)}{t\tau_\varepsilon} \right] + \frac{f(t) - f(0)}{t^\alpha} \right\}. \quad (9)$$

However, as the fractional order  $\alpha$  approaches 1, the Beta distribution becomes increasingly concentrated near 0, potentially introducing significant numerical errors due to this treatment.

Therefore, in [31, 32], the authors propose a new method Improved MCfPINNs using Gauss-Jacobi quadrature. These methods approximate the integral in equation (8) using a weighted sum over carefully selected quadrature points  $(w_i, \tau_i)_{i=1}^N$  (see detailed forms in [35]), resulting in the approximation:

$$\partial_t^\alpha f(t) \approx \frac{1}{\Gamma(1 - \alpha)} \left\{ \alpha t^{1-\alpha} \left( \sum_{i=1}^M w_i \frac{f(t) - f(t - t\tau_i)}{t\tau_i} \right) + \frac{f(t) - f(0)}{t^\alpha} \right\} \quad (10)$$

The rapid convergence of Gauss-Jacobi quadrature [36] significantly accelerates training, as it allows for a smaller number of quadrature points  $M$  compared to the Monte Carlo approach when  $\alpha < 1$ . These promising results naturally motivate the extension of this strategy to the case  $\alpha > 1$ , which we explore in this work.

### 3. Transformed MCfPINNs

This section presents the main proposed methods. Specifically, we first extend the MCfPINNs concept based on Monte Carlo and Gauss-Jacobi from  $\alpha \in (0, 1)$  to  $\alpha \in (1, 2)$  directly. Subsequently, we present a novel transformed approach for approximating the fractional derivative  $\partial^\alpha f$  with  $\alpha \in (1, 2)$ , and validate its effectiveness through numerical integration using both Monte Carlo sampling and Gauss-Jacobi quadrature. Monte Carlo integration can be interpreted as a form of numerical quadrature, where both the sampling nodes and their corresponding weights are derived from a probability density function. In this sense, the quadrature points correspond to the sampling nodes used in both Monte Carlo integration and the Gauss-Jacobi method.

For clarity, we denote by  $M$  the number of quadrature points used in either the Monte Carlo or Gauss-Jacobi approach, collectively referred to as numerical integration schemes throughout this work.

#### 3.1. Transformed MCfPINNs for $\alpha \in (1, 2)$

Lemma 2.1 gives an alternative representation of Caputo fractional derivatives of arbitrary orders  $\alpha$ , which can be directly extended to the case  $\alpha \in (1, 2)$ .

However, a direct application of this result to solve the diffusion-wave equation (1) introduces practical challenges due to the presence of the first-order derivatives within the integral term. Specifically, evaluating  $\partial^\alpha f(t_i)$  at points  $\{t_i\}_{i=1}^N$  using  $M$  quadrature points  $\{\tau_j\}_{j=1}^M$  requires computing the first-order derivative  $f'(t_i - t_i\tau_j)$  a total of  $O(MN)$  times. This results in substantial computational overhead, particularly when leveraging automatic differentiation frameworks on GPUs. In contrast, for the case  $\alpha \in (0, 1)$ , the evaluation involves only  $f(t_i - t_i\tau_j)$  without differentiation, significantly reducing the computational burden and making the approach more amenable to PINNs.

To address this challenge, we propose an integrand transformation formulation derived from Lemma 2.1, aimed at mitigating the cost associated with repeated evaluation of first-order derivatives. The core idea is to reformulate the representation to eliminate the explicit dependence on  $f'(t - t\tau)$  within the integral term. The following theorem represents the transformed representation:

**Theorem 3.1.** *According to Lemma 2.1, let  $n = 2$  and suppose  $f$  is sufficiently smooth, then*

$$\begin{aligned} \partial_t^\alpha f(t) &= \frac{1}{\Gamma(2-\alpha)} \int_0^t (t-\tau)^{1-\alpha} f^{(2)}(\tau) d\tau \\ &= \frac{1}{\Gamma(2-\alpha)} \left\{ \frac{f'(t) - f'(0)}{t^{\alpha-1}} + (\alpha-1)t^{2-\alpha} \int_0^1 \frac{f'(t) - f'(t-t\tau)}{t\tau} \tau^{1-\alpha} d\tau \right\} \end{aligned} \quad (11)$$

$$= \frac{1}{\Gamma(2-\alpha)} \left\{ \frac{f'(t) - f'(0)}{t^{\alpha-1}} - (\alpha-1) \frac{f(t) - f(0) - tf'(t)}{t^\alpha} - \alpha(\alpha-1)t^{2-\alpha} \int_0^1 \frac{f(t) - f(t-t\tau) - t\tau f'(t)}{(t\tau)^2} \tau^{1-\alpha} d\tau \right\}. \quad (12)$$

*Proof.* According to the proof in [34, Lemma 2.10], if  $f$  is sufficiently smooth, we have the fact from Taylor expansion that

$$\lim_{\tau \rightarrow t^-} (f'(t) - f'(\tau))(t-\tau)^{1-\alpha} = 0, \quad \lim_{\tau \rightarrow t^-} (f(t) - f(\tau) - (t-\tau)f'(t))(t-\tau)^{-\alpha} = 0 \quad (13)$$

Then from equation (2) ( $n = 2$ ), we obtain from integration by parts that

$$\begin{aligned}
\Gamma(2 - \alpha)\partial_t^\alpha f &= \int_0^t (t - \tau)^{1-\alpha} f^{(2)}(\tau) d\tau \\
&= f'(\tau)(t - \tau)^{1-\alpha}|_0^t - (\alpha - 1) \int_0^t (t - \tau)^{-\alpha} f'(\tau) d\tau \\
&= -(f'(t) - f'(0))(t - \tau)^{1-\alpha}|_0^t + f'(t)(t - \tau)^{1-\alpha}|_0^t - (\alpha - 1) \left[ f(\tau)(t - \tau)^{-\alpha}|_0^t - \alpha \int_0^t (t - \tau)^{-\alpha-1} f(\tau) d\tau \right] \\
&= (f'(t) - f'(0))t^{1-\alpha} + f'(t)(t - \tau)^{1-\alpha}|_0^t - (\alpha - 1) \left[ f(\tau)(t - \tau)^{-\alpha}|_0^t - \alpha \int_0^t (t - \tau)^{-\alpha-1} f(\tau) d\tau \right] \\
&= I_1 + I_2 - (\alpha - 1)I_3
\end{aligned}$$

with the first limit in (13). For  $I_3$ , we use integration by parts again, given  $\lim_{\tau \rightarrow t^-} (f(t) - f(\tau) - (t - \tau)f'(\tau))(t - \tau)^{-\alpha} = 0$ , we have

$$\begin{aligned}
I_3 &= -(f(t) - f(\tau) - (t - \tau)f'(\tau))(t - \tau)^{-\alpha}|_0^t + (f(t) - (t - \tau)f'(\tau))(t - \tau)^{-\alpha}|_0^t - \alpha \int_0^t (t - \tau)^{-\alpha-1} f(\tau) d\tau \\
&= (f(t) - f(0) - tf'(\tau))t^{-\alpha} - f'(t)(t - \tau)^{1-\alpha}|_0^t + \alpha \int_0^t (t - \tau)^{-\alpha-1} (f(t) - f(\tau)) d\tau,
\end{aligned}$$

then

$$\begin{aligned}
I_2 - (\alpha - 1)I_3 &= -(\alpha - 1)(f(t) - f(0) - tf'(\tau))t^{-\alpha} + \alpha f'(t)(t - \tau)^{1-\alpha}|_0^t - (\alpha - 1)\alpha \int_0^t (t - \tau)^{-\alpha-1} (f(t) - f(\tau)) d\tau \\
&= II_1 + II_2.
\end{aligned}$$

Consider  $II_2$ ,

$$\begin{aligned}
II_2 &= \alpha(\alpha - 1)f'(t) \int_0^t (t - \tau)^{-\alpha} d\tau - (\alpha - 1)\alpha \int_0^t (t - \tau)^{-\alpha-1} (f(t) - f(\tau)) d\tau \\
&= -\alpha(\alpha - 1) \int_0^t (t - \tau)^{-\alpha-1} (f(t) - f(\tau) - (t - \tau)f'(\tau)) d\tau.
\end{aligned}$$

In general, we would have

$$\begin{aligned}
\Gamma(2 - \alpha)\partial_t^\alpha f &= (I_1 + I_2 - (\alpha - 1)I_3) = \frac{1}{\Gamma(2 - \alpha)}(I_1 + II_1 + II_2) \\
&= (f'(t) - f'(0))t^{1-\alpha} - (\alpha - 1)(f(t) - f(0) - tf'(\tau))t^{-\alpha} - \alpha(\alpha - 1) \int_0^t (t - \tau)^{-\alpha-1} (f(t) - f(\tau) - (t - \tau)f'(\tau)) d\tau.
\end{aligned}$$

□

Based on the transformation in Theorem 3.1, we reformulate the numerical integrations as follows:

**Corollary 3.1.** *According to Theorem 3.1, we could obtain two types of numerical approximations  $\bar{\partial}_\tau^\alpha f(t)$  for  $\partial_t^\alpha f$  with  $\alpha \in (1, 2)$ .*

- **Type I: direct form.** *From (11), if we directly use the information from the first derivative of  $f$ , the numerical integrations based on Monte Carlo approach or Gauss-Jacobi quadrature could be written as:*

– **Monte Carlo(MC-I):**

$$\partial_t^\alpha f(t) \approx \bar{\partial}_\tau^\alpha f(t) = \frac{1}{\Gamma(2 - \alpha)} \left\{ \frac{f'(t) - f'(0)}{t^{\alpha-1}} + \frac{(\alpha - 1)}{(2 - \alpha)} t^{2-\alpha} \mathbb{E}_{\tau \sim \text{Beta}(2-\alpha, 1)} \left[ \frac{f'(t) - f'(t - t\tau)}{t\tau^\alpha} \right] \right\}. \quad (14)$$

– **Gauss Jacobi(GJ-I):**

$$\partial_t^\alpha f(t) \approx \bar{\partial}_\tau^\alpha f(t) = \frac{1}{\Gamma(2-\alpha)} \left\{ \frac{f'(t) - f'(0)}{t^{\alpha-1}} + (\alpha-1)t^{2-\alpha} \left( \sum_{i=1}^M w_i \frac{f'(t) - f'(t-t\tau_i)}{t\tau_i} \right) \right\}. \quad (15)$$

- **Type II: transformed form.** Alternatively, using the transformed expression in (12), which avoids computing first-order derivatives at shifted points, we obtain:

– **Monte Carlo(MC-II):**

$$\begin{aligned} \partial_t^\alpha f(t) \approx \bar{\partial}_\tau^\alpha f(t) &= \frac{1}{\Gamma(2-\alpha)} \left\{ \frac{f'(t) - f'(0)}{t^{\alpha-1}} - (\alpha-1) \frac{f(t) - f(0) - tf'(t)}{t^\alpha} \right. \\ &\quad \left. - \frac{\alpha(\alpha-1)}{(2-\alpha)} t^{2-\alpha} \mathbb{E}_{\tau \sim \text{Beta}(2-\alpha, 1)} \left[ \frac{f(t) - f(t-t\tau) - t\tau f'(t)}{(t\tau_\varepsilon)^2} \right] \right\}. \end{aligned} \quad (16)$$

– **Gauss Jacobi(GJ-II):**

$$\begin{aligned} \partial_t^\alpha f(t) \approx \bar{\partial}_\tau^\alpha f(t) &= \frac{1}{\Gamma(2-\alpha)} \left\{ \frac{f'(t) - f'(0)}{t^{\alpha-1}} - (\alpha-1) \frac{f(t) - f(0) - tf'(t)}{t^\alpha} \right. \\ &\quad \left. - \alpha(\alpha-1)t^{2-\alpha} \left( \sum_{i=1}^M w_i \frac{f(t) - f(t-t\tau_i) - t\tau_i f'(t)}{(t\tau_i)^2} \right) \right\}. \end{aligned} \quad (17)$$

The form (**Type I**) arises as a direct extension of the results in Section 2.2, where we implicitly treat the Caputo derivative as  $\partial_t^\alpha f(t) = \partial_t^{\alpha-1}(\partial_t f)$  for  $\alpha - 1 \in (0, 1)$ . The key distinction between the direct form (**Type I**) and the transformed form (**Type II**) lies in the presence of the shifted derivative term  $f'(t - t\tau)$ . As previously discussed, in the context of PINNs, computing such derivatives at shifted points using automatic differentiation is computationally expensive, particularly on GPUs. Therefore, we aim to avoid evaluating  $f'(t - t\tau)$  unless strictly necessary. By contrast, the transformed formulation (**Type II**) eliminates this term, potentially reducing the computational burden. Moreover, consistent with empirical observations reported in [31, 32], Gauss-Jacobi quadrature tends to outperform Monte Carlo integration in both accuracy and convergence rate. This motivates the initial hypothesis that the **GJ-II** scheme offers the most favorable trade-off, combining high numerical accuracy with lower computational cost. However, this hypothesis will be critically examined in the following sections through detailed experimental analysis.

### 3.2. Numerical Validation of Integrand Transformation

In this subsection, we validate the numerical performance of the four computational schemes introduced in Corollary 3.1. Our primary focus is on examining their behavior under varying values of  $\alpha \in (1, 2)$  and different numbers of quadrature points  $M$ .

**Example 3.1.** From [34, Example 2.4], given  $f(t) = e^{\lambda t}$ ,  $\lambda \in \mathbb{R}$ , we have

$$\partial_t^\alpha f(t) = \lambda^2 t^{2-\alpha} E_{1,3-\alpha}(\lambda t),$$

here  $E_{\alpha,\beta}(t)$  is the Mittag-Leffler functions (see details in [37, 34]).

**Various  $M$ .** We begin by examining the impact of the number of quadrature points  $M$  on the accuracy for the four numerical methods to compute Caputo derivatives. Specifically, we fix  $\alpha = 1.5$ ,  $\lambda = -1.0$ ,  $t = 0.75$ ,  $\varepsilon = 10^{-10}$  for **MC-I**,  $\varepsilon = 10^{-7}$  for **MC-II**. We consider a range of quadrature sizes, with  $M \in \{2^k \times 10\}_{k=1}^{10}$  for Monte Carlo method and  $M \in \{2^k \times 10\}_{k=1}^3$  for Gauss-Jacobi quadrature, then compute the relative errors

$$err = |\partial_t^\alpha f(t) - \bar{\partial}_\tau^\alpha f(t)| / |\partial_t^\alpha f(t)|$$

as shown in Figure 1. For the Monte Carlo methods, increasing  $M$  results in a reduction of the relative error, reflecting the expected convergence behavior of stochastic integration. However, for Gauss-Jacobi quadrature, increasing  $M$

beyond a moderate size is not always beneficial. Specifically, we use the function `roots_jacobi` from SciPy package to compute the quadrature points and weights. When  $M$  becomes large, numerical inaccuracies in computing the roots of Jacobi polynomials may degrade the quality of the quadrature rule. Despite this, we observe that the relative errors of the Gauss-Jacobi method are substantially smaller than those of the Monte Carlo approach, even with fewer quadrature points. These results highlight the superior accuracy and efficiency of Gauss-Jacobi quadrature in this setting.

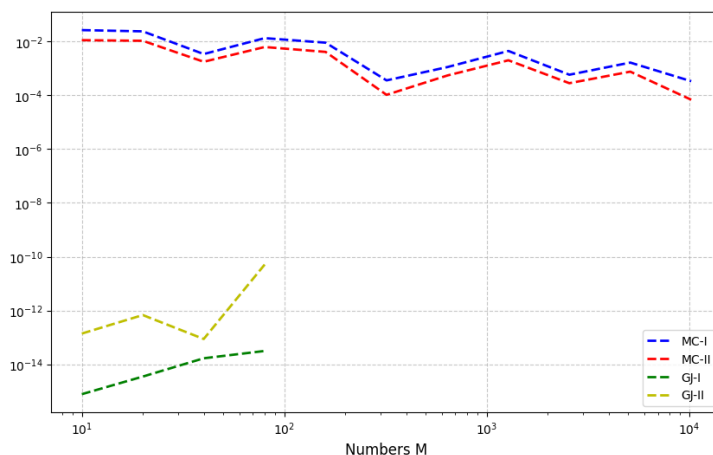


Figure 1: Relative errors of  $\bar{\partial}_t^\alpha f(t)$  in Example 3.1 different number of quadrature points for different numerical integration methods.

**Various  $\alpha$  with sufficient quadrature points.** In this experiment, we investigate the numerical behavior of each method as the fractional order  $\alpha$  varies, while maintaining a sufficiently larger number of quadrature points to ensure convergence. Specifically, we set  $M = 10000$  for Monte Carlo methods and  $M = 100$  for Gauss-Jacobi methods. We fix  $t = 1.5$ ,  $\lambda = -1.0$ , and use  $\varepsilon = 10^{-10}$  for **MC-I** and  $\varepsilon = 10^{-7}$  for **MC-II**. We assign  $\alpha$  values from 100 equidistant nodes within the interval  $(1.01, 1.99)$ .

The results, presented in Figure 2, indicate that as the fractional order  $\alpha$  approaches 2, the accuracy of Monte Carlo methods deteriorates markedly. This degradation occurs because the probability density function becomes more singular, causing samples to cluster near 0. Consequently, the introduction of  $\varepsilon$  leads to significant discrepancies in Monte Carlo integration, while its omission results in numerical instabilities. Therefore, the Gauss-Jacobi method emerges as the more robust alternative.

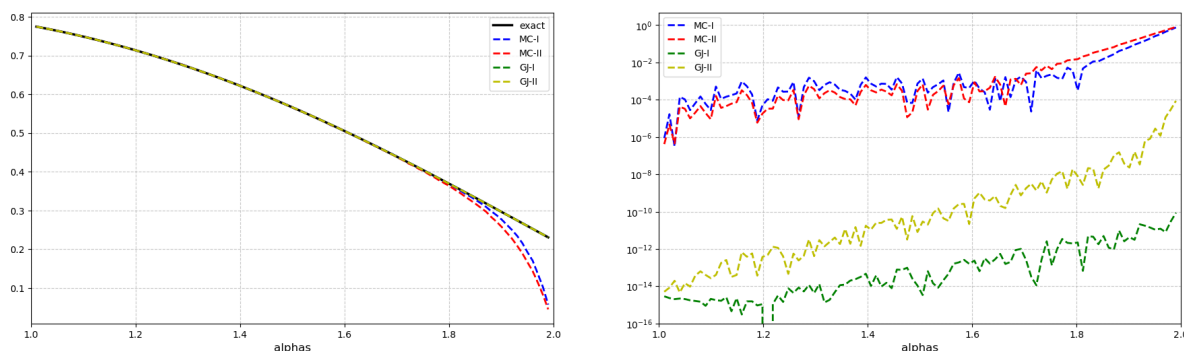


Figure 2: Solution profiles of  $\bar{\partial}_t^\alpha f(t)$  of Example 3.1 with different  $\alpha$  for numerical integration methods. Left: the computed  $\bar{\partial}_t^\alpha f(t)$  for each method, *exact* means the true  $\partial_t^\alpha f(t)$ . Right: the relative errors *err* for each method.

The numerical results validate the effectiveness of our intergrand transformation (**Type II**). When comparing the Monte Carlo and Gauss-Jacobi approaches, we observe that the Gauss-Jacobi quadratures consistently exhibit superior

performance, especially as  $\alpha$  approaches 2. This improvement is primarily attributed to the sensitivity of the Monte Carlo method to the hyperparameter setting of  $\varepsilon$ , which becomes increasingly critical due to the singular behavior of the integrand near zero in this regime.

The comparison of computational costs is presented in Section 4 within the PINNs framework, where we detail the training time required for each numerical integration method. Our proposed tDWfPINNs achieve a substantial reduction in both computation time and GPU resource consumption, indicating a notable gain in computational efficiency. While the Gauss-Jacobi method generally outperforms the Monte Carlo approach, special care must be taken in selecting an appropriate number of quadrature points to balance computational efficiency and approximation accuracy.

## 4. Experiments

In this section, we use transformed MCfPINNs in Section 3 to solve time-fractional partial differential equations with  $\alpha \in (1, 2)$ . In the following we use **MC-I**, **MC-II**, **GJ-I**, **GJ-II** referring to the four numerical integrations in Corollary 3.1.

To further improve the training performance, we adopt a resampling strategy as described in [27]. This approach consists of iterative training cycles, each involving a fixed number of training epochs followed by a resampling of collocation points in the domain. The resampling strategy significantly enhances the convergence behavior of the neural network by mitigating the risk of stagnation in local minima, a common challenge in the training of PINNs. Through this adaptive sampling, the network is better guided toward learning the underlying solution dynamics, particularly in regions with high approximation errors.

Unless otherwise specified, we adopt the following settings in all numerical experiments. The neural network architecture consists of 7 hidden layers, each with 20 neurons, and employs the hyperbolic tangent  $\tanh$  as the activation function. This choice ensures that Theorem 3.1 and Corollary 3.1 can be applied directly to the smooth neural network solution  $u(t, \mathbf{x}; \theta)$ . For the Monte Carlo methods, the setting of  $\varepsilon$  of **MC-I** is  $10^{-10}$  and **MC-II**  $10^{-7}$ . To measure the accuracy of the learned solutions, we use the  $L^2$  relative error defined as

$$e_r(\theta) = \frac{\sqrt{\sum_{i=1}^n [u(t_i, \mathbf{x}_i; \theta) - u^*(t_i, \mathbf{x}_i)]^2}}{\sqrt{\sum_{i=1}^N [u^*(t_i, \mathbf{x}_i)]^2}}, \quad (18)$$

where  $(t_i, \mathbf{x}_i)$ ,  $i = 1, 2, \dots, N$  represents the test data set. All trainings and tests are conducted on Nvidia V100 32G.

### 4.1. Summary of results and findings

In this section, we summarize our numerical observations across various problem settings. We picture the performance of our proposed methods after training, examine solution behaviors, and explore the limitations of PINNs when applied to time-fractional diffusion-wave equations.

Regarding computational efficiency, our proposed tDWfPINNs significantly reduce both time consumption and GPU resource usage, while preserving a comparable level of accuracy. This makes the transformed numerical scheme highly recommended for time-fractional PDEs with orders  $\alpha \in (1, 2)$ .

Furthermore, the Gauss-Jacobi method typically requires significant fewer quadrature points than the Monte Carlo method to achieve similar accuracy (as demonstrated in Section 4.2). This indicates the potential superiority of the Gauss-Jacobi integration in certain contexts. However, we observe that the wave component introduced by the Mittag-Leffler functions can strongly influence the numerical behavior of both the Gauss-Jacobi quadrature and Monte Carlo method. While our experiments consistently favor the Gauss-Jacobi method, its effectiveness is sensitive to the choice of quadrature resolution. Careful tuning of the number of quadrature points is therefore essential to fully exploit its advantages without incurring instability or excessive computational overhead.

Finally, we conduct numerical experiments on time-fractional Burgers equations with  $\alpha \in (1, 2)$  and incorporate the RAD method from [26]. Unlike the significant improvements RAD provides for integer-order equations, its application in tDWfPINNs yields only marginal improvements. This limited benefit persists even in cases where RAD successfully identifies shock formations in the solution. We hypothesize that this phenomenon stems from the intrinsic wave-like nature of diffusion-wave equations, which introduces complex nonlocal behaviors not present in

classical integer-order models. These observations point to the need for further investigation into the interplay between adaptive sampling techniques and the nonlocal memory effects of fractional dynamics.

#### 4.2. Time-fractional diffusion-wave equations in 1D domain

In the warm-up stage we consider the following TFPDEs in  $\Omega = (0, 1)$  with  $\alpha = 1.5$ :

$$\begin{aligned} \partial_t^\alpha u(t, x) - u_{xx}(t, x) &= 0, \quad (t, \mathbf{x}) \in (0, 1] \times \Omega, \\ u(t, 0) = u(t, 1) &= 0, \quad t \in (0, 1], \\ u(0, x) &= 2 \sin(\pi x), \quad x \in \Omega, \\ \partial_t u(0, x) &= -\sin(\pi x), \quad x \in \Omega, \end{aligned} \tag{19}$$

with exact solution

$$u(t, x) = (2E_{\alpha,1}(-\pi^2 t^\alpha) - tE_{\alpha,2}(-\pi^2 t^\alpha)) \sin(\pi x)$$

here  $E_{\alpha,\beta}(t)$  is the Mittag-Leffler functions (see details in [37, 34]).

The exact solution is depicted in Figure 3. In contrast to (sub)diffusion equations, the solution of the diffusion-wave equation exhibits a distinctive wave-like structure, primarily driven by the Mittag-Leffler functions. This characteristic introduces additional complexity, making such equations potentially more difficult to solve using vanilla PINNs compared to (sub)diffusion equations. To assess the computational performance of the numerical integration methods presented in Corollary 3.1, we conducted extensive tests with results summarized in Table 1.

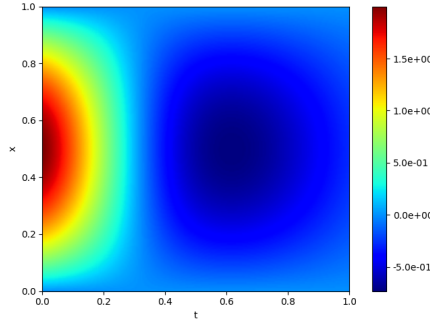


Figure 3: Solution profiles of  $u(t, x)$  in equation (19).

For small batches, we sampled 5000 collocation points within the domain, along with 1000 points each on the spatial and temporal boundaries. In the large-batch setting, we increased the sampling density to 10000 points in the domain and 2000 points on both the spatial and temporal boundaries. We set the maximum number of iterations to be  $L = 10$ , with each iteration comprising 5000 epochs trained using the Adam optimizer at a learning rate of  $10^{-3}$ . The weighting parameter in the loss function (6) was set to 1.0.

Regarding computational efficiency, our analysis reveals that the integrand transformation exhibit significantly lower and more stable computation times compared to their direct counterparts (**MC-I** and **GJ-I**), which demonstrate rapidly increasing computational costs. For each value of  $M$  (number of quadrature points), the integrand transformation consistently require substantially less computational time than direct methods even for  $M = 16$  of Gauss-Jacobi method, our proposed method could save several seconds over 5000 epochs. Additionally, the memory usage is markedly reduced. For instance, with small batches at  $M = 1280$ , **MC-II** consumes only 10.5GB of GPU memory, whereas **MC-I** requires 29.1GB. This reduced memory footprint enables the transformed MCfPINNs to accommodate denser sampling points and larger  $M$  within a single GPU environment. Importantly, these gains in efficiency come without sacrificing numerical accuracy; both integration types maintain comparable error levels.

Moreover, the Gauss-Jacobi quadrature method appears to offer computational advantages over the Monte Carlo approach, as it requires fewer quadrature points to achieve comparable levels of accuracy, further reinforcing its suitability for efficient and precise fractional-order computations.

In the following, we present solution profiles derived from the results in Table 1. We first compare the cases of the Monte Carlo method in Figure 4, which displays the solution profiles and absolute errors for each numerical method.

Cases	Small batches		Large batches			Small batches		Large batches	
$M$ /Type	MC-I	MC-II	MC-I	MC-II	$M$ /Type	GJ-I	GJ-II	GJ-I	GJ-II
$M = 80$	1.12e-1 5m37s	7.69e-2 4m06s	1.12e-1 8m55s	6.16e-2 5m22s	$M = 16$	3.60e-2 3m09s	2.62e-2 2m57s	4.38e-2 3m37s	3.80e-2 3m19s
$M = 160$	1.10e-1 8m51s	5.76e-2 5m17s	1.09e-1 15m34s	8.61e-2 8m38s	$M = 32$	3.92e-2 3m24s	2.93e-2 3m01s	3.93e-2 5m06s	3.28e-2 3m39s
$M = 320$	8.20e-2 15 m33s	4.11e-2 8m34s	9.67e-2 24m02s	4.44e-2 10m52s	$M = 48$	3.05e-2 4m12s	4.83e-2 3m21s	4.82e-2 6m19s	6.01e-2 4m13s
$M = 640$	6.20e-2 23m58s	3.84e-2 10m48s	7.94e-2 45m10s	5.54e-2 19m45s	$M = 64$	4.87e-2 5m02s	4.46e-2 3m34s	3.21e-2 7m38s	3.78e-2 4m35s
$M = 1280$	7.0e-2 45m10s	5.82e-2 19m44s	OoM	5.64e-2 37m25s	$M = 80$	4.56e-2 5m33s	3.72e-2 3m56s	5.35e-2 8m50s	3.66e-2 5m17s

Table 1:  $L^2$  relative error and computational time of equation (19) with different  $M$  and number of points. For each grid, the first row is the relative error, the second row is the average computational time for 5000 epochs. OoM means out of memory.

The results indicate that improved accuracy in the computation of fractional derivatives leads to more effective training outcomes. At relatively low values of  $M$ , the Monte Carlo methods suffer from reduced accuracy, emphasizing the advantage of Gauss-Jacobi methods in achieving better performance with fewer quadrature points. This highlights the superior computational efficiency of Gauss-Jacobi quadratures in practice.

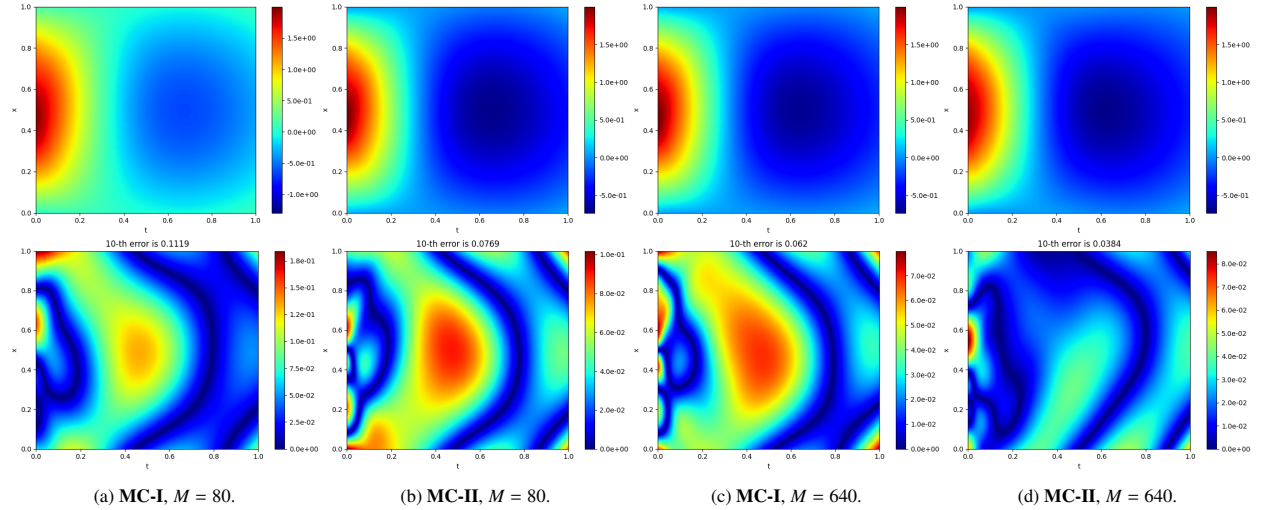


Figure 4: Profiles of absolute error and neural network solutions for equation (19) with Monte Carlo method for  $M = 80$  and  $M = 640$ . First row: numerical solutions. Second row: absolute error.

However, the Gauss-Jacobi quadrature method demonstrates remarkable efficiency in terms of the number of quadrature points required. As illustrated in Figure 5, which compares solution profiles and absolute error distributions for implementations with  $M = 16$  and  $M = 80$ , the method achieves comparable accuracy levels with significantly fewer quadrature points.

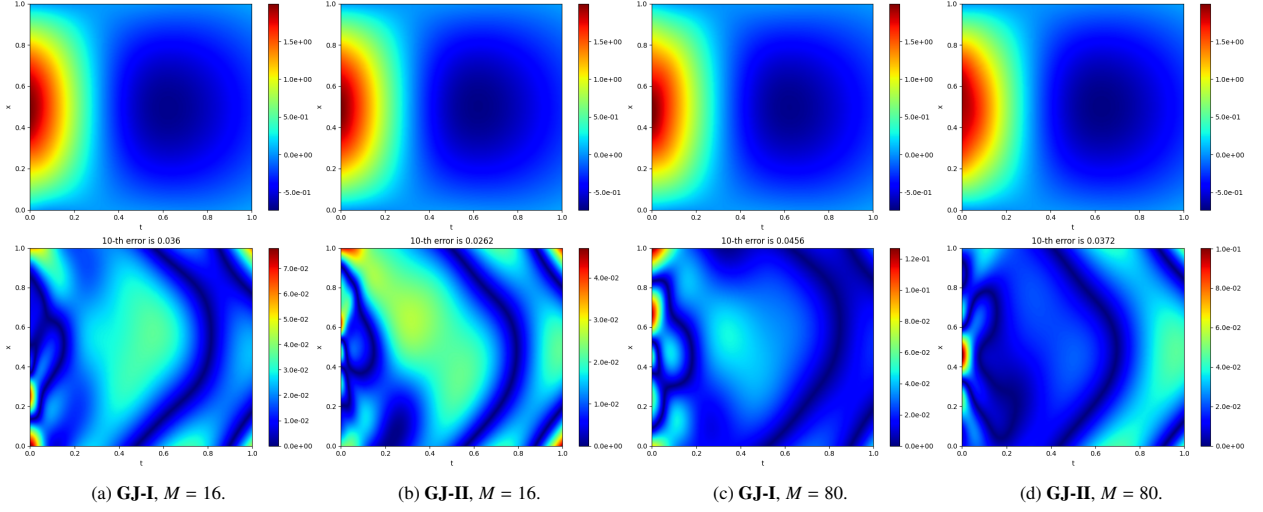


Figure 5: Profiles of absolute error and neural network solutions for equation (19) with Gauss-Jacobi method for  $M = 16$  and  $M = 80$ . First row: numeral solutions. Second row: absolute error.

#### 4.3. Time-fractional Diffusion-Wave equation with adjusted parameters

Here we consider the following TFPDEs in  $\Omega = (0, 1)$ :

$$\begin{aligned}
 \partial_t^\alpha u(t, x) - \frac{\lambda}{k^2 \pi^2} u_{xx}(t, x) &= 0, \quad (t, \mathbf{x}) \in (0, T] \times \Omega, \quad \lambda \in \mathbb{R}^+, \quad k \in \mathbb{N}, \\
 u(t, 0) = u(t, 1) &= 0, \quad t \in (0, 1], \\
 u(0, x) &= \sin(k\pi x), \quad x \in \Omega, \\
 \partial_t u(0, x) &= -0.5 \sin(k\pi x), \quad x \in \Omega,
 \end{aligned} \tag{20}$$

with exact solution

$$u(t, x) = (E_{\alpha,1}(-\lambda t^\alpha) - 0.5tE_{\alpha,2}(-\lambda t^\alpha)) \sin(k\pi x).$$

The equation (19) can be regarded as a special case with  $\lambda = \pi^2$ ,  $k = 1$ , scaled initial conditions, and  $T = 1$ . In Table 2, the final time is set to  $T = 2$ . Small batches, consistent with those in subsection 4.2, are adopted. The training procedure is configured with a maximum of  $L = 3$  iterations, each consisting of 5000 epochs and optimized using the Adam optimizer with a learning rate of 0.001. The exact solutions for each case and each  $\alpha$  are presented in Figure 6, allowing a clear comparison of the diffusion and wave components in the solutions. As  $\alpha$  increases, the wave component becomes more pronounced, while larger values of the diffusion coefficient  $\lambda/(k^2\pi^2)$  enhance the influence of the diffusion effects. This interplay between the wave and diffusion components helps explain the numerical behaviors observed in the subsequent results.

We show the relative errors and the time consumption in Table 2 with numerical integrations of different  $M$ . The proposed tDWfPINNs demonstrate accuracy on par with direct numerical integration methods, while significantly reducing computational time. These extensive numerical experiments further validate the efficiency of our approach in solving the time-fractional diffusion-wave equation.

As the training process for PINNs progresses, our experiments consistently demonstrate that the Gauss-Jacobi method outperforms the Monte Carlo approach. However, we observe that the performance of both methods tends to deteriorate as the equation parameter increases implying the increasing of solution complexities.

Examining Table 2, we observe that for cases involving larger values of  $\lambda$  and  $k$ , models with higher fractional order  $\alpha$  tend to produce more accurate results than those with smaller  $\alpha$ . This trend is likely attributable to the strong decay in the Mittag-Leffler scaling factor for small  $\alpha$  when  $\lambda$  is large, as demonstrated in Figure 6.

For further elucidate this behavior, Figure 7 presents the absolute error distributions of MC-II and GJ-II for cases with  $k = 2, \lambda = 4$  and  $k = 4, \lambda = 4$ , evaluated across various  $\alpha$  values when  $M = 640$  and  $M = 80$ . The

		$k = 1, \lambda = 1$		$k = 2, \lambda = 4$			$k = 1, \lambda = 1$		$k = 2, \lambda = 4$	
$\alpha$		<b>MC-I</b>	<b>MC-II</b>	<b>MC-I</b>	<b>MC-II</b>		<b>GJ-I</b>	<b>GJ-II</b>	<b>GJ-I</b>	<b>GJ-II</b>
1.25	$M = 80$	2.16e-2 5m38s	3.15e-2 4m04s	4.58e-2 5m39s	4.63e-2 3m59s	$M = 16$	5.80e-3 3m13s	1.03e-2 2m51s	4.74e-2 3m11s	7.06e-2 3m01s
	$M = 640$	1.93e-2 24m00s	1.10e-2 10m52s	6.75e-2 23m57s	7.68e-2 10m50s	$M = 80$	7.10e-3 5m31s	7.60e-3 4m01s	6.32e-2 5m35s	6.07e-2 3m53s
1.5	$M = 80$	3.83e-2 5m36s	8.50e-3 4m06s	6.51e-2 5m36s	4.75e-2 3m52s	$M = 16$	1.20e-2 3m08s	1.14e-2 2m59s	3.24e-2 3m07s	4.21e-2 3m01s
	$M = 640$	4.35e-2 23m55s	2.35e-2 10m49s	5.13e-2 23m56s	3.15e-2 10m53s	$M = 80$	6.10e-3 5m31s	1.82e-2 4m04s	2.74e-2 5m31s	3.39e-2 3m49s
1.75	$M = 80$	7.20e-3 5m32s	7.10e-3 4m05s	6.39e-2 5m34s	2.59e-2 3m54s	$M = 16$	4.1e-3 3m15s	2.40e-3 3m00s	1.64e-2 3m07s	2.00e-2 2m59s
	$M = 640$	4.50e-3 24m02s	1.74e-2 10m52s	2.64e-2 23m58s	4.50e-2 10m52s	$M = 80$	1.19e-2 5m32s	8.90e-3 4m00s	1.82e-2 5m31s	1.52e-2 3m55s
		$k = 4, \lambda = 4$		$k = 6, \lambda = 6$			$k = 4, \lambda = 4$		$k = 6, \lambda = 6$	
1.25	$M = 80$	5.69e-2 5m39s	3.91e-2 3m59s	1.52e-1 5m39s	2.98e-1 3m54s	$M = 16$	6.34e-2 3m07s	6.23e-2 2m59s	1.09e-1 3m03s	9.56e-2 3m00s
	$M = 640$	2.76e-2 23m59s	6.16e-2 10m48s	1.01e-1 23m53s	1.22e-1 10m52s	$M = 80$	3.80e-2 5m36s	8.00e-2 4m02s	1.04e-1 5m31s	1.20e-1 4m01s
1.5	$M = 80$	4.64e-2 5m41s	3.94e-2 4m06s	6.41e-2 5m33s	5.68e-2 4m10s	$M = 16$	3.60e-2 3m07s	3.96e-2 3m00s	4.69e-2 3m05s	5.41e-2 2m56s
	$M = 640$	4.65e-2 23m52s	2.75e-2 10m54s	8.74e-2 23m54s	5.28e-2 10m54s	$M = 80$	2.84e-2 5m33s	2.40e-2 3m57s	4.29e-2 5m39s	8.75e-2 4m07s
1.75	$M = 80$	9.74e-2 5m35s	3.78e-2 3m55s	6.10e-2 5m42s	8.12e-2 4m05s	$M = 16$	7.48e-2 3m07s	3.37e-2 3m02s	5.45e-2 3m05s	3.44e-2 2m59s
	$M = 640$	2.59e-2 23m58s	3.00e-2 10m50s	5.28e-2 23m55s	6.71e-2 10m52s	$M = 80$	3.62e-2 5m31s	1.47e-2 3m54s	4.76e-2 5m30s	1.99e-2 4m04s

Table 2: Results of different numerical integrations with different parameters in equation (20). In each grid, the first row is the  $L^2$  relative error, the second row is the consuming time for each case within 5000 epochs.

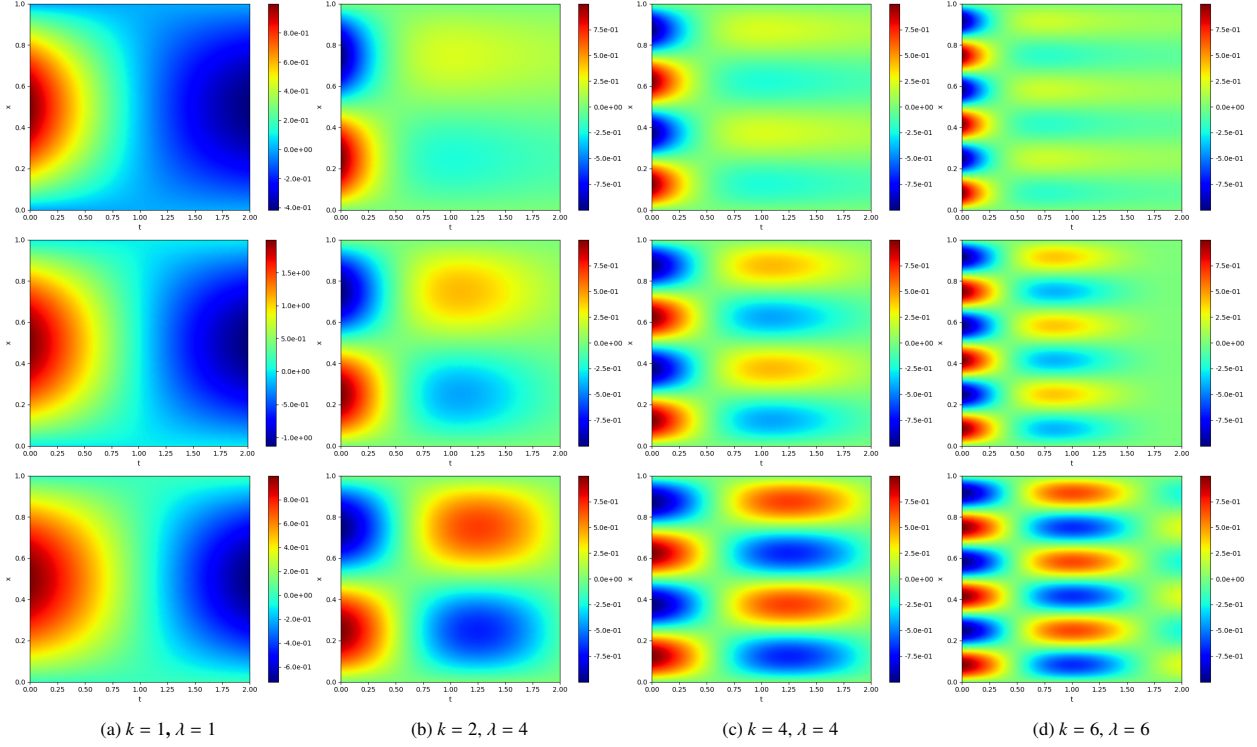


Figure 6: Exact solution of cases in Table 2 with different  $\alpha$ ,  $k$  and  $\lambda$ . In the first row,  $\alpha = 1.25$ , in the second row,  $\alpha = 1.5$ , in the third row,  $\alpha = 1.75$ .

error patterns revealed in this figure lead to two significant observations. First, the error patterns obtained using the Gauss-Jacobi method tend to exhibit higher frequency content than those from the Monte Carlo method. This is indicative of a more effective representation of the underlying solution features and aligns with theoretical insights derived from neural tangent kernel analysis, such as those presented in [25]. Second, significant error concentrations are consistently observed near the initial temporal layer and spatial boundaries. This suggests that the design of future training strategies—such as boundary-focused sampling or adaptive loss weighting—should prioritize these regions to improve overall approximation quality.

In the following experiments, the number  $M$  is fixed at 80, and we always use our integrand transformation. This choice is motivated by earlier findings demonstrating that the transformed methods attain comparable accuracy to their direct counterparts while significantly reducing computational overhead.

To further investigate the observed performance discrepancies among different configurations, we conducted extended training experiments with sufficient iterations. Specifically, for the cases presented in Table 2, comprehensive training was implemented using the Adam optimizer with a learning rate of  $10^{-5}$  and  $L = 50$ . The corresponding numerical outcomes are documented in Table 3. With adequate training, both methods demonstrate enhanced solution accuracy when  $\lambda$  is relatively small; however, as  $\lambda$  increases, performance degradation becomes evident, highlighting the influence of the diffusion component on solution scaling. The Gauss-Jacobi method consistently outperforms the Monte Carlo approach under these extended training conditions. This suggests that for smaller  $M$ , the Monte Carlo integration lacks sufficient resolution to capture solution features effectively, leading to suboptimal training convergence. Consequently, when employing Monte Carlo-based integration within PINNs, a significantly larger number of quadrature samples is advisable to ensure acceptable accuracy. Figure 8 illustrates the absolute errors, revealing that the error patterns of **GJ-II** continue to present the high-frequency error structure, implying the better resolution of the Gauss-Jacobi method.

Extensive numerical experiments demonstrate that both parameters of the Mittag-Leffler function  $E_{\alpha,\beta}(-\lambda t^\alpha)$  significantly influence the performance of PINNs. Specifically,  $\lambda$  characterizes the decay properties of the solution, while

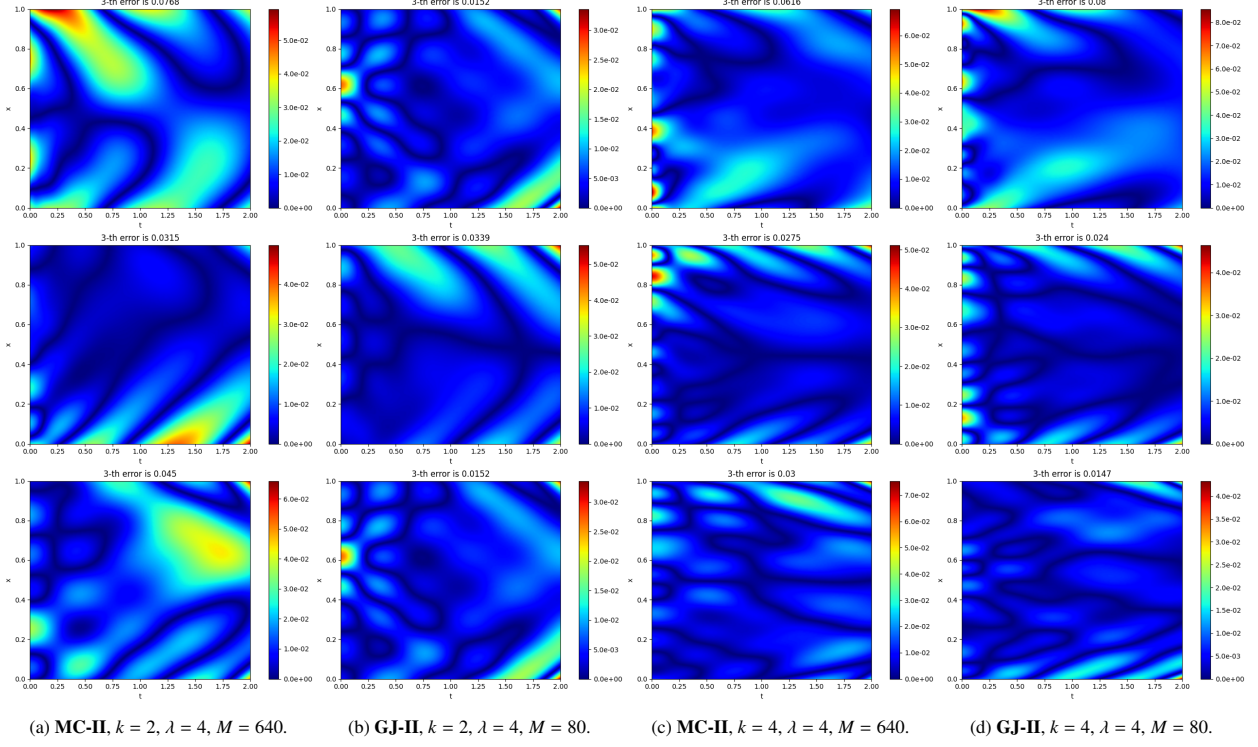


Figure 7: Absolute errors of cases in Table 2 with different  $\alpha$ ,  $k$  and  $\lambda$ . In the first row,  $\alpha = 1.25$ , in the second row,  $\alpha = 1.5$ , in the third row,  $\alpha = 1.75$ .

	$k = 1, \lambda = 1$		$k = 2, \lambda = 4$	
	MC-II	GJ-II	MC-II	GJ-II
$\alpha = 1.25$	3.90e-3	2.80e-3	2.91e-2	2.58e-2
$\alpha = 1.5$	4.00e-3	1.90e-3	3.41e-2	1.79e-2
$\alpha = 1.75$	5.40e-3	2.40e-3	2.96e-2	1.17e-2
	$k = 4, \lambda = 4$		$k = 6, \lambda = 6$	
$\alpha = 1.25$	3.68e-2	2.29e-2	7.11e-2	7.30e-2
$\alpha = 1.5$	3.26e-2	1.20e-2	8.75e-2	2.00e-2
$\alpha = 1.75$	3.16e-2	1.37e-2	7.45e-2	1.87e-2

Table 3: Relative errors under sufficient training with  $L = 50$  and learning rate  $10^{-5}$ .

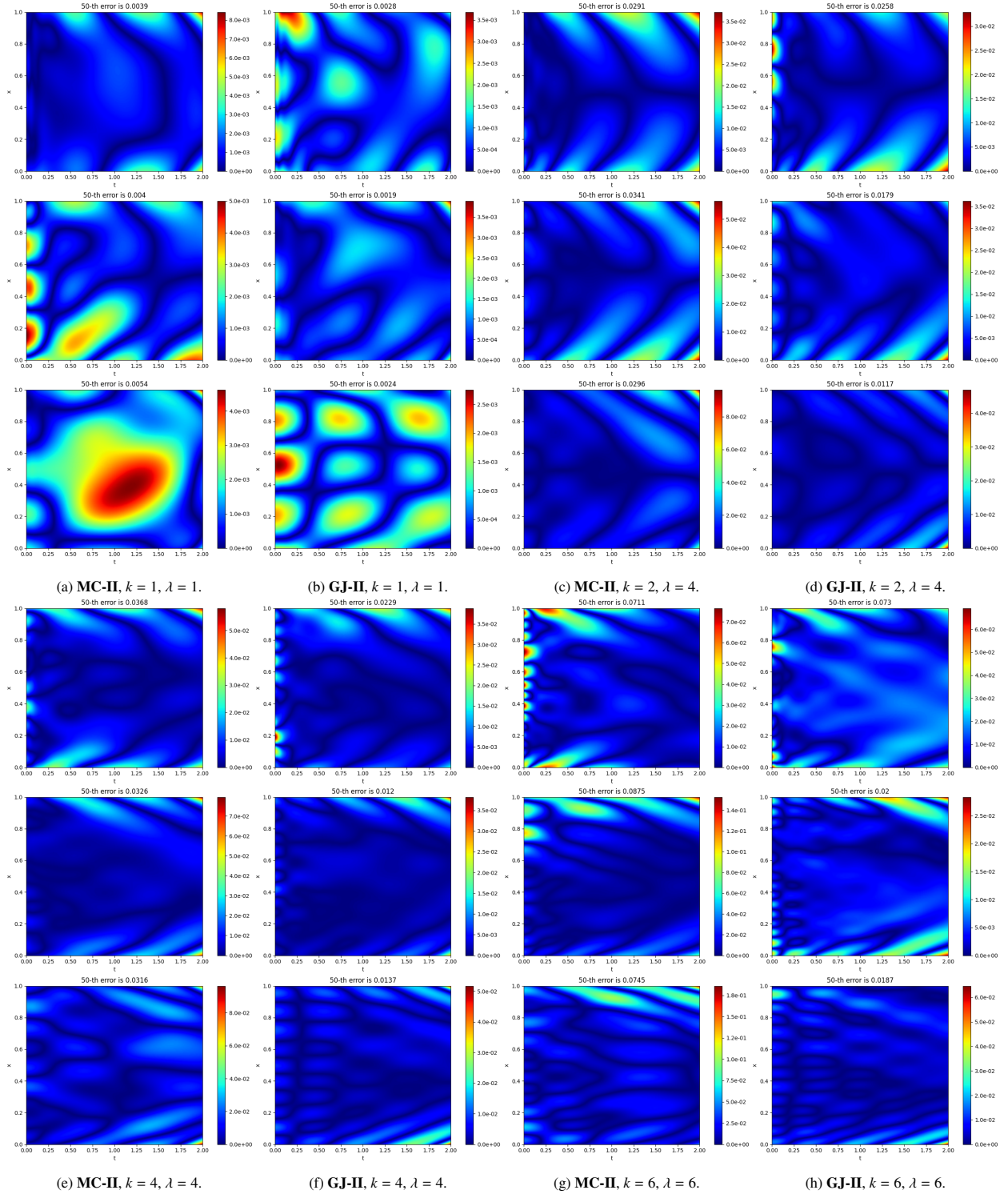


Figure 8: Absolute errors of cases in Table 3 with sufficient trainings of different  $\alpha$ ,  $k$  and  $\lambda$ . For each sub-figure, in the first row,  $\alpha = 1.25$ , in the second row,  $\alpha = 1.5$ , in the last row  $\alpha = 1.75$ .

$\alpha$  governs its wave-like characteristics. Larger values of  $\lambda$  lead to more rapid solution decay, which can degrade the fidelity of the learned solution. Conversely, increasing  $\alpha$  tends to counteract this decay effect by enhancing the wave component, thereby improving the overall solution quality. This behavior is reflected in our numerical results, where models trained with  $\alpha = 1.75$  consistently outperform those with  $\alpha = 1.25$ , particularly in scenarios involving large  $\lambda$ . In this investigation, we focus on the effects of  $\lambda$  and  $\alpha$  while maintaining a fixed final time  $T = 2$ , thereby isolating these parameters from temporal influences.

As both  $\lambda$  and  $\alpha$  increase, the complexity of the solution dynamics imposes greater challenges on the training process. Notably, as  $\alpha$  approaches 2, the performance of the Monte Carlo-based method degrades significantly. This degradation is attributed to sensitivity with respect to the hyperparameter  $\varepsilon$ , as discussed previously in Section 3.2. While increases in  $\lambda$  negatively affect the accuracy of all tested methods, the Gauss-Jacobi approach demonstrates superior robustness, particularly for larger values of  $\alpha$ , where the mitigated decay yields more stable solution representations.

These findings highlight the necessity of selecting an appropriate quadrature strategy—either Gauss-Jacobi or Monte Carlo—based on the specific parameter regimes characterizing the problem. The choice of numerical integration method plays a critical role in the efficiency and accuracy of PINN training, especially in the context of time-fractional partial differential equations.

A series of experiments were performed for different values of  $\alpha$ . Figure 9 presents the numerical errors for  $\alpha \in [1.1, 1.9]$  using both Monte Carlo and Gauss-Jacobi methods under various  $k$  and  $\lambda$  settings. As  $\lambda$  increases, the numerical performance deteriorates across all methods. When  $\alpha$  goes to 2, the performance of Monte Carlo method deteriorate primarily due to the hyperparameter setting  $\varepsilon$ .

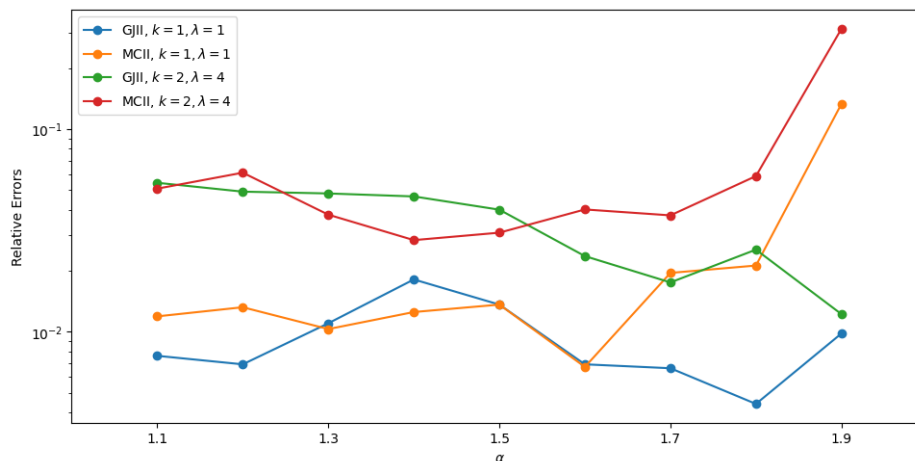


Figure 9: Relative errors of MC-II and GJ-II with different  $\alpha$  for  $k = 1, \lambda = 1$  and  $k = 2, \lambda = 4$ .

Furthermore, we conducted additional experiments with a fixed  $k = 2$  and varying decay parameter  $\lambda$  for  $\alpha \in 1.25, 1.5, 1.75$ . The results are illustrated in Figure 10. These experiments reveal that increasing the decay parameter  $\lambda$  substantially impacts the numerical performance of both integration methods. For special case of GJ-II with  $\alpha = 1.75$ , with the slow decay of the exact solution, PINNs could still simulate the solution under satisfactory.

Additionally, we examine the influence of parameter  $k$  on solution behavior with fixed  $\lambda = 1.0$  to isolate it from the effects of large  $\lambda$  values on numerical performance. The results, presented in Figure 11, indicate that as  $k$  increases substantially, solution accuracy slightly deteriorates, suggesting the need for enhanced training strategies when dealing with large  $k$  values.

In general, the Mittag-Leffler function embedded within the solution of the time-fractional diffusion-wave equation presents significant training challenges. The parameter  $\lambda$ , which typically originates from the eigenvalue component of the spatial operator and characterizes the decay behavior of the solution, exerts a relatively major influence on the solution behavior for both Monte Carlo and Gauss-Jacobi methods due to the fast decay of the solution. Conversely, the parameter  $\alpha$ , which derives from the time-fractional component of the temporal differential operator and governs

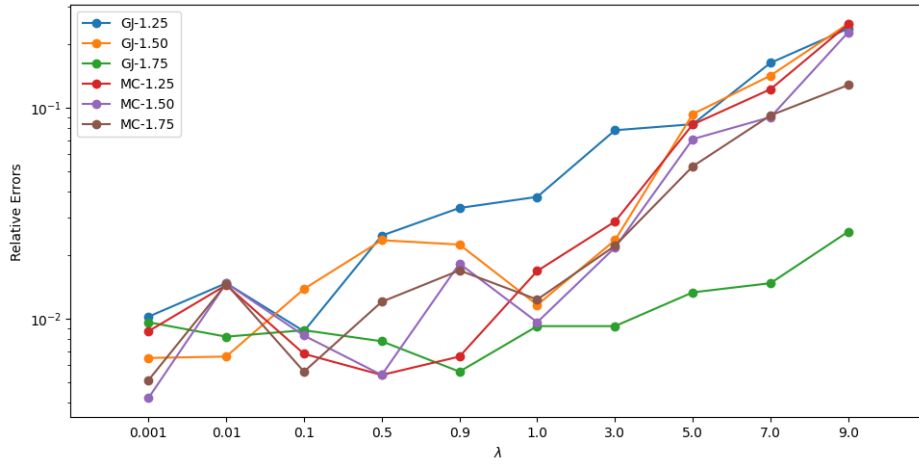


Figure 10: Relative errors of MC-II and GJ-II with different  $\lambda$  for  $k = 2$ ,  $\alpha \in \{1.25, 1.5, 1.75\}$ .

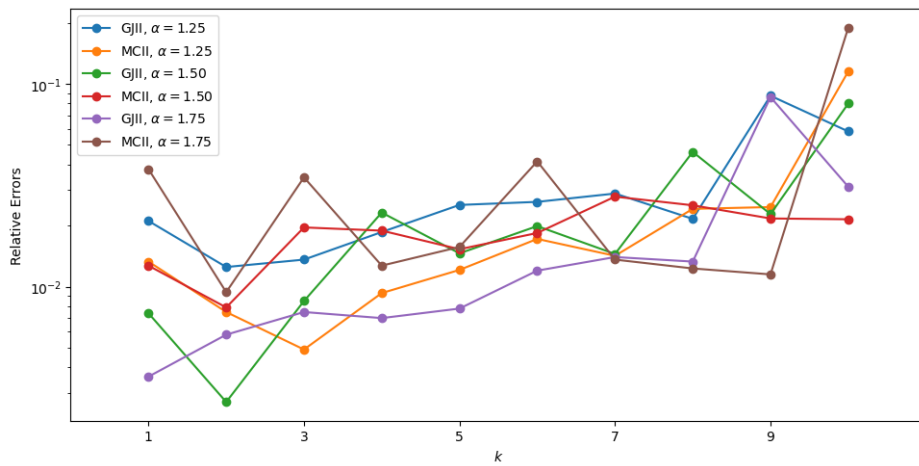


Figure 11: Relative errors of MC-II and GJ-II with different  $k$  for  $\lambda = 1$ ,  $\alpha \in \{1.25, 1.5, 1.75\}$ .

the wave characteristics of the solution, substantially influence the solution behavior for Monte Carlo method due to hyperparameter  $\varepsilon$  when  $\alpha$  approaches 2, but not for Gauss-Jacobi method. Large  $\alpha$  would enhance the wave characteristics of the solution, delay the solution decay, so it could help for PINNs to simulate the solution.

It is important to highlight that the main challenges in training time-fractional diffusion-wave equations are closely related to the broader issue of training PINNs for wave equations. For future work, relevant insights can be drawn from the published results in [25, 38].

#### 4.4. Time-fractional Burgers equation with $\alpha \in (1, 2)$

In this subsection we consider the time-fractional Burgers equation with  $\alpha \in (1, 2)$ , showed as

$$\begin{aligned} \partial_t^\alpha u + uu_x &= \frac{0.01}{\pi} u_{xx}, \text{ in } \Omega \times (0, T], \\ u &= 0, \text{ on } \partial\Omega, \\ u(0) &= -\sin(\pi x), \partial_t u(0) = \sin(\pi x), \text{ in } \Omega, \end{aligned} \quad (21)$$

where  $\Omega = (-1, 1)$ ,  $T = 1$ .

Building upon the analysis presented in Section 4.3, we observe that the wave component establishes a dynamic equilibrium with the diffusion component of the solution. This phenomenon is particularly evident in the fractional Burgers equation when examining different  $\alpha$ . Figure 12 illustrates the exact solution profiles for two representative cases:  $\alpha = 1.1$  and  $\alpha = 1.8$ . The results clearly demonstrate that shock formation is progressively delayed as  $\alpha$  increases, providing further evidence of the complex interplay between diffusive and wave-like behaviors in diffusion-wave systems.

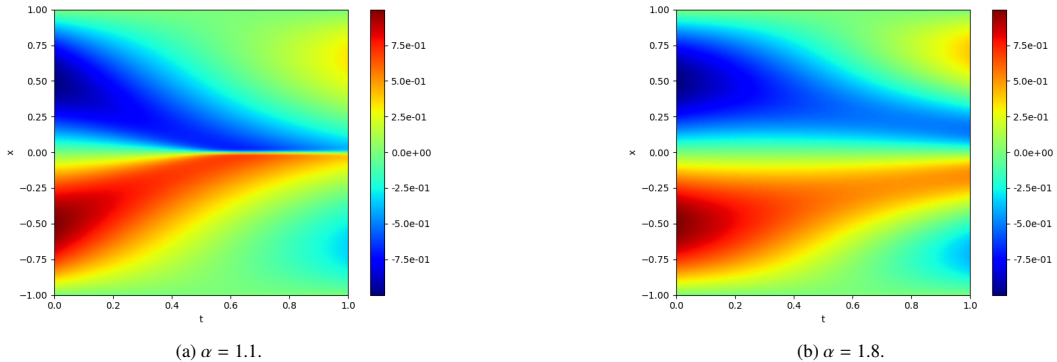


Figure 12: Exact solutions of Burgers equation (21) with  $\alpha = 1.1$  and  $\alpha = 1.8$ .

In the following experiments, we employ a minimal dataset comprising 1500 collocation points within the domain and 500 points along the spatial and temporal boundaries, the Adam learning rate is 0.0001, we train 10000 epochs with the max iterations  $L = 20$ . The initial loss weight is set to  $\lambda_{init} = 100$ . We implement the RAD method for adaptive sampling as proposed by [26]. We set the adaptive resampling ratios be 0.3, e.g., in each iteration we substitute 30% of the points with RAD sampling points in the domain. Our evaluation of the RAD application focuses on three key metrics: relative errors, maximum absolute errors, and the frequency distribution of absolute error patterns.

Throughout these experiments, we utilize our integration transformation as the default computational approach with  $M = 80$ , based on our findings that these methods can achieve comparable accuracy with significantly reduced computational costs. Based on the findings presented in Section 4.3, we demonstrate a clear preference for the Gauss-Jacobi method (**GJ-II**) over the Monte Carlo method (**MC-II**).

Figure 13 presents the numerical solutions and associated error distributions for the case where  $\alpha = 1.1$ , comparing different numerical integration methods. The results demonstrate that the Gauss-Jacobi method achieves significantly higher accuracy in solution approximation compared to the Monte Carlo method. For the Monte Carlo method (**MC-II**), our analysis reveals that while the RAD approach does not significantly reduce relative errors, it effectively

decreases the maximum ( $L^\infty$ ) errors and enhances the frequency distribution of error patterns. This behavior indicates that RAD helps the optimization process escape local minima during training. In contrast, for the Gauss-Jacobi method (**GJ-II**), the implementation of RAD yields minimal improvement in numerical performance, revealing that the application of adaptive sampling in time-fractional Burgers equations requires specialized enhancement.

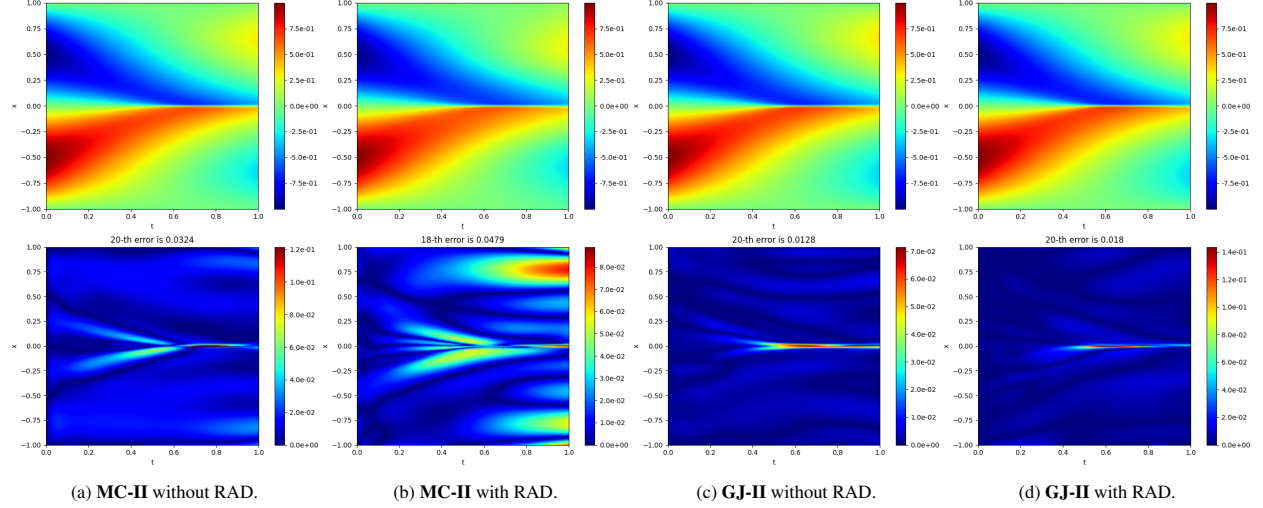


Figure 13: Profiles of absolute error and neural network solutions for Burgers equation (21) at  $\alpha = 1.1$ . First row: numeral solutions. Second row: absolute error.

Figure 14 illustrates the distribution of collocation points sampled by the RAD method at different training stages. Our analysis reveals a distinct pattern in the sampling distribution: during the initial training phases, the loss function predominantly concentrates on regions near the temporal boundary ( $t = 0$ ) and shock formation zones. As training progresses, however, the spectral characteristics of the loss function exhibit increased frequency components, causing the RAD method to redistribute its sampling focus across a broader domain.

Notably, this behavior differs significantly from RAD's performance in integer-order Burgers equations (see details in [27]). In the fractional-order case, even when the adaptive sampling correctly identifies shock regions, the PINNs struggle to achieve satisfactory training outcomes due to the inherent wave component in the solution structure. This observation suggests that effective training strategies for fractional-order Burgers equations should prioritize accurately capturing the wave characteristics of the solution before addressing the shock regions that arise from the nonlinear advection term in the Burgers equation.

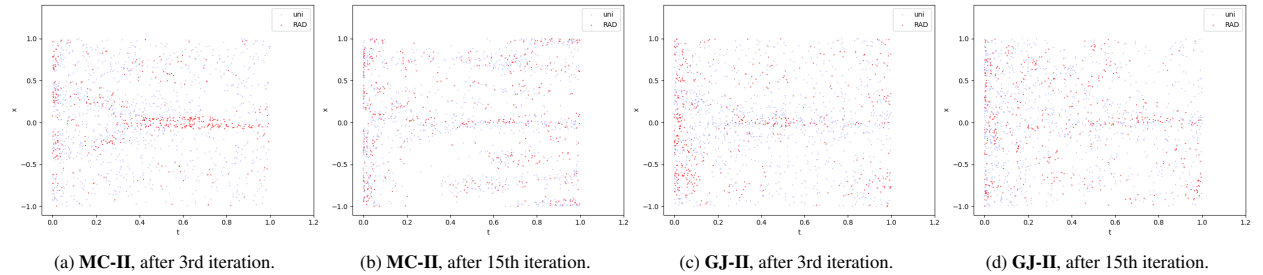


Figure 14: Profiles of node distributions for Burgers equation (21) with  $\alpha = 1.1$ .

For the case where  $\alpha = 1.8$ , Figure 15 demonstrates that PINNs generate satisfactory numerical approximations, primarily because shock formation does not occur before the terminal time  $T = 1$ . When implementing the RAD methodology with the Monte Carlo integration approach (**MC-II**), we observe a significant enhancement in solution accuracy, with maximum absolute errors reduced by approximately 50% compared to the standard implementation without adaptive sampling. Interestingly, this performance improvement is not working for Gauss-Jacobi method.

For the **GJ-II** method, the application of RAD actually yields inferior numerical results compared to the uniform sampling. This contrasting behavior further substantiates our earlier findings regarding the sensitivity of Gauss-Jacobi method to wave-dominated regimes when  $\alpha > 1.5$ . A notably large absolute error is observed near the spatial boundary  $x = -1$  when using the **GJ-II** method with RAD, which may be attributed to the choice of the weighting parameter in equation (6). For potential improvements, one may refer to adaptive weighting strategies proposed in [39, 38].

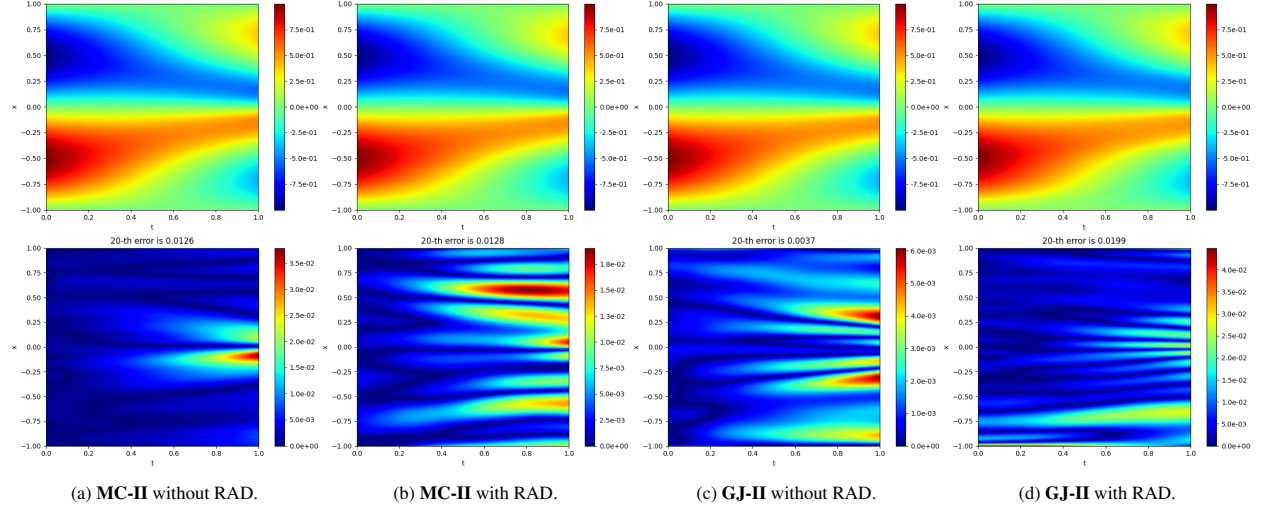


Figure 15: Profiles of absolute error and neural network solutions for Burgers equation (21) at  $\alpha = 1.8$ . First row: numeral solutions. Second row: absolute error.

The distinct numerical behaviors observed when applying the RAD to Monte Carlo and Gauss-Jacobi integration methods can be directly attributed to the fundamental influence of adaptive sampling on the optimization landscape. Figure 16 illustrates the distribution of sampling points at both early and final training stages. For both methods, RAD effectively concentrates computational resources in critical regions near the temporal boundaries ( $t = 0$  and  $t = T$ ), where the PINNs must accurately approximate the initial condition near  $t = 0$  and anticipate potential shock formation near  $t = T$ .

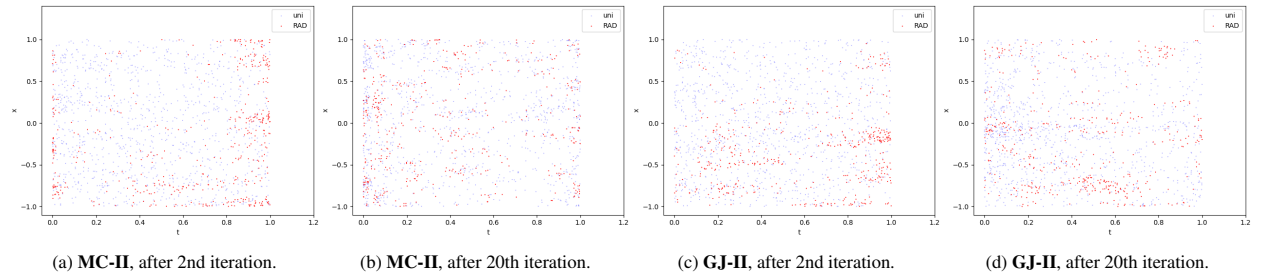


Figure 16: Profiles of node distributions for Burgers equation (21) with  $\alpha = 1.8$ .

The numerical behaviors observed across these experiments align with our expectations. The RAD methodology demonstrates significant efficacy in addressing problems characterized by solution singularities, effectively redistributing computational datasets to critical regions. However, while the Gauss-Jacobi method generally outperforms the Monte Carlo approach, PINNs still face challenges in focusing on shock regions when the wave component in the solution structure is significant. This highlights the need for specialized techniques when applying adaptive sampling frameworks to time-fractional Burgers equations with  $\alpha \in (1, 2)$ .

These findings lead to an important conclusion regarding numerical approaches for time-fractional derivatives: mesh-free numerical integration techniques offer substantially greater flexibility than their mesh-based counterparts

for specific problem classes. The capacity to incorporate adaptive sampling strategies represents a significant advantage of these mesh-free approaches, enabling efficient resolution of complex solution features without the constraints imposed by fixed discretization schemes. However, the unique properties of time-fractional diffusion-wave equations, which exhibit both diffusive and wave-like behaviors, require careful consideration when applying some advanced training strategies like adaptive sampling methods, adaptive weighting methods and see more details in [38, 25].

## 5. Conclusion and future works

In this paper, we proposed the transformed Diffusion-Wave fractional Physics-Informed Neural Networks (tD-WfPINNs), a novel and efficient computational approach for solving time-fractional diffusion-wave problems with order  $\alpha \in (1, 2)$ . Our work contributes several key advancements to the numerical treatment of fractional differential equations within the PINNs paradigm.

The main contribution is the development of a transformed technique for computing the fractional derivative with order  $\alpha \in (1, 2)$  that avoids differentiation at quadrature points. This transformation represents a significant advancement over direct numerical methods, as demonstrated by our comprehensive numerical experiments. The proposed tDWfPINNs method achieved comparable accuracy to direct numerical approaches while significantly reducing both computation time and memory usage, enabling the handling of larger sampling points and higher  $M$  values on a single GPU.

Our comparative analysis of Monte Carlo and Gauss-Jacobi approaches across various time-fractional partial differential equations revealed important insights into their respective performance characteristics. While Gauss-Jacobi quadratures require fewer quadrature points to achieve comparable accuracy at lower  $M$  values, our findings indicate that the choice between Monte Carlo and Gauss-Jacobi methods requires careful consideration of the wave components in solutions. Specifically, the Gauss-Jacobi method demonstrated superior performance, and we need to set some regularization hyperparameters in Monte Carlo method appropriately when  $\alpha$  goes to 2.

We successfully integrated our method with the Residual-based Adaptive Distribution (RAD) framework and applied it to the time-fractional Burgers equation. The numerical experiments reveal that the choice between Monte Carlo and Gauss-Jacobi integration approaches must be made judiciously, depending on the fractional order  $\alpha$ , to ensure optimal performance.

Despite the promising results, several challenges remain in applying tDWfPINNs to time-fractional diffusion-wave equations. For the Gauss-Jacobi method, it is crucial to compute quadrature points and weights with sufficient accuracy, particularly when using larger values of  $M$  to maintain high precision. For the Monte Carlo method, careful consideration of hyperparameter settings becomes essential when  $\alpha$  approaches 2. Most importantly, specialized training methods should be considered when applying PINNs to time-fractional diffusion-wave equations, as these equations uniquely exhibit both diffusive and wave-like behaviors that require tailored numerical approaches.

Several promising directions remain for future exploration. First, we aim to establish a theoretical framework for analyzing the behavior of PINNs when applied to time-fractional diffusion-wave equations, with the goal of uncovering underlying mechanisms responsible for the observed performance. Second, we plan to enhance the training efficiency and robustness of the tDWfPINNs framework by incorporating advanced strategies developed for PINNs, such as [38, 25]. Third, we intend to extend our framework to inverse problems, which are prevalent in scientific and engineering applications involving time-fractional PDEs with  $\alpha \in (1, 2)$ . The proposed tDWfPINNs, with their improved computational efficiency, offer a promising foundation for addressing challenges in parameter estimation and system identification in such inverse settings.

In conclusion, the proposed tDWfPINNs method represents a significant advancement in the efficient numerical solution of time-fractional diffusion-wave equations, offering a promising framework for tackling complex fractional-order systems across various scientific and engineering applications.

## CRedit authorship contribution statement

**Zhengqi Zhang:** Writing–review & editing, Writing – original draft, Visualization, Validation, Software, Methodology, Investigation, Formal analysis, Data curation. **Jing Li:** Writing – review & editing, Supervision, Project administration, Methodology, Funding acquisition, Conceptualization.

## Declaration of competing interest

The authors declare that they have no known competing financial interests or personal relationships that could have appeared to influence the work reported in this paper.

## Data availability

The code in this work is available from the GitHub repository <https://github.com/Zenki229/tMcfPINN>.

## References

- [1] F. Mainardi, Fractional relaxation-oscillation and fractional diffusion-wave phenomena, *Chaos, Solitons & Fractals* 7 (9) (1996) 1461–1477. doi:10.1016/0960-0779(95)00125-5.
- [2] F. Mainardi, *Fractional calculus and waves in linear viscoelasticity*, second edition Edition, World Scientific, New Jersey, 2022, literaturverzeichnis: Seite 433-581.
- [3] S. Swain, S. Swain, B. Panda, M. C. Tripathy, Modeling and optimal analysis of lung cancer cell growth and apoptosis with fractional-order dynamics, *Computers in Biology and Medicine* 188 (2025) 109837. doi:10.1016/j.combiomed.2025.109837.
- [4] M. BenSalah, S. Tatar, S. Ulusoy, Bayesian inference for a time-fractional hiv model with nonlinear diffusion (Mar. 2025). arXiv:2503.23638, doi:10.48550/ARXIV.2503.23638.
- [5] R. Metzler, J. Klafter, The random walk's guide to anomalous diffusion: a fractional dynamics approach, *Physics Reports* 339 (1) (2000) 1–77. doi:10.1016/s0370-1573(00)00070-3.
- [6] R. Metzler, J.-H. Jeon, A. G. Cherstvy, E. Barkai, Anomalous diffusion models and their properties: non-stationarity, non-ergodicity, and ageing at the centenary of single particle tracking, *Phys. Chem. Chem. Phys.* 16 (44) (2014) 24128–24164. doi:10.1039/c4cp03465a.
- [7] K. Sakamoto, M. Yamamoto, Initial value/boundary value problems for fractional diffusion-wave equations and applications to some inverse problems, *Journal of Mathematical Analysis and Applications* 382 (1) (2011) 426–447. doi:10.1016/j.jmaa.2011.04.058.
- [8] H. Jiang, F. Liu, I. Turner, K. Burrage, Analytical solutions for the multi-term time-fractional diffusion-wave/diffusion equations in a finite domain, *Computers & Mathematics with Applications* 64 (10) (2012) 3377–3388. doi:10.1016/j.camwa.2012.02.042.
- [9] O. P. Agrawal, Solution for a fractional diffusion-wave equation defined in a bounded domain, *Nonlinear Dynamics* 29 (1/4) (2002) 145–155. doi:10.1023/a:1016539022492.
- [10] R. Du, W. Cao, Z. Sun, A compact difference scheme for the fractional diffusion-wave equation, *Applied Mathematical Modelling* 34 (10) (2010) 2998–3007. doi:10.1016/j.apm.2010.01.008.
- [11] Z.-z. Sun, *Fractional differential equations*, De Gruyter, Berlin, 2020.
- [12] E. Cuesta, C. Lubich, C. Palencia, Convolution quadrature time discretization of fractional diffusion-wave equations, *Mathematics of Computation* 75 (254) (2006) 673–696. doi:10.1090/s0025-5718-06-01788-1.
- [13] B. Jin, B. Li, Z. Zhou, Correction of high-order bdf convolution quadrature for fractional evolution equations, *SIAM Journal on Scientific Computing* 39 (6) (2017) A3129–A3152. doi:10.1137/17m1118816.
- [14] H. Zhu, C. Xu, A fast high order method for the time-fractional diffusion equation, *SIAM Journal on Numerical Analysis* 57 (6) (2019) 2829–2849. doi:10.1137/18m1231225.
- [15] M. Stynes, E. O’Riordan, J. L. Gracia, Error analysis of a finite difference method on graded meshes for a time-fractional diffusion equation, *SIAM Journal on Numerical Analysis* 55 (2) (2017) 1057–1079. doi:10.1137/16m1082329.
- [16] S. Chen, J. Shen, Z. Zhang, Z. Zhou, A spectrally accurate approximation to subdiffusion equations using the log orthogonal functions, *SIAM Journal on Scientific Computing* 42 (2) (2020) A849–A877. doi:10.1137/19m1281927.
- [17] M. Zayernouri, G. E. Karniadakis, Fractional Sturm–Liouville eigen-problems: Theory and numerical approximation, *Journal of Computational Physics* 252 (2013) 495–517. doi:10.1016/j.jcp.2013.06.031.
- [18] M. Raissi, P. Perdikaris, G. Karniadakis, Physics-informed neural networks: A deep learning framework for solving forward and inverse problems involving nonlinear partial differential equations, *Journal of Computational Physics* 378 (2019) 686–707. doi:10.1016/j.jcp.2018.10.045.
- [19] S. Cai, Z. Mao, Z. Wang, M. Yin, G. E. Karniadakis, Physics-informed neural networks (pinns) for fluid mechanics: a review, *Acta Mechanica Sinica* 37 (12) (2021) 1727–1738. doi:10.1007/s10409-021-01148-1.
- [20] S. Cuomo, V. S. Di Cola, F. Giampaolo, G. Rozza, M. Raissi, F. Piccialli, Scientific machine learning through physics-informed neural networks: Where we are and what’s next, *Journal of Scientific Computing* 92 (3) (Jul. 2022). doi:10.1007/s10915-022-01939-z.
- [21] G. Pang, L. Lu, G. E. Karniadakis, fpinns: Fractional physics-informed neural networks, *SIAM Journal on Scientific Computing* 41 (4) (2019) A2603–A2626. doi:10.1137/18m1229845.
- [22] B. Lu, Z.-p. Hao, C. Moya, G. Lin, Fpinn-deeponet: An operator learning framework for multi-term time-fractional mixed diffusion-wave equations (2025). doi:10.2139/ssrn.5080263.
- [23] Y. Vats, M. Mehra, D. Oelz, A. K. Singh, A new perspective for scientific modelling: Sparse reconstruction-based approach for learning time-space fractional differential equations, *Journal of Computational and Nonlinear Dynamics* 19 (12) (Sep. 2024). doi:10.1115/1.4066330.
- [24] H. Ren, X. Meng, R. Liu, J. Hou, Y. Yu, A class of improved fractional physics informed neural networks, *Neurocomputing* 562 (2023) 126890. doi:10.1016/j.neucom.2023.126890.
- [25] S. Wang, X. Yu, P. Perdikaris, When and why pinns fail to train: A neural tangent kernel perspective, *Journal of Computational Physics* 449 (2022) 110768. doi:10.1016/j.jcp.2021.110768.
- [26] C. Wu, M. Zhu, Q. Tan, Y. Kartha, L. Lu, A comprehensive study of non-adaptive and residual-based adaptive sampling for physics-informed neural networks, *Computer Methods in Applied Mechanics and Engineering* 403 (2023) 115671. doi:10.1016/j.cma.2022.115671.

- [27] Z. Zhang, J. Li, B. Liu, Annealed adaptive importance sampling method in pinns for solving high dimensional partial differential equations, *Journal of Computational Physics* 521 (2025) 113561. [doi:10.1016/j.jcp.2024.113561](https://doi.org/10.1016/j.jcp.2024.113561).
- [28] T. Zhang, D. Zhang, S. Shi, Z. Guo, Spectral-fpinns: spectral method based fractional physics-informed neural networks for solving fractional partial differential equations, *Nonlinear Dynamics* 113 (11) (2025) 12565–12588. [doi:10.1007/s11071-025-11067-6](https://doi.org/10.1007/s11071-025-11067-6).
- [29] Z. Chen, C. QIU, Z. Li, Laplace-based physics-informed neural networks for solving nonlinear coefficient inverse problem for acoustic equation with fractional derivative (2025). [doi:10.2139/ssrn.5142405](https://doi.org/10.2139/ssrn.5142405).
- [30] L. Guo, H. Wu, X. Yu, T. Zhou, Monte carlo fpinns: Deep learning method for forward and inverse problems involving high dimensional fractional partial differential equations, *Computer Methods in Applied Mechanics and Engineering* 400 (2022) 115523. [doi:10.1016/j.cma.2022.115523](https://doi.org/10.1016/j.cma.2022.115523).
- [31] Z. Hu, K. Kawaguchi, Z. Zhang, G. E. Karniadakis, Tackling the curse of dimensionality in fractional and tempered fractional pdes with physics-informed neural networks, *Computer Methods in Applied Mechanics and Engineering* 432 (2024) 117448. [doi:10.1016/j.cma.2024.117448](https://doi.org/10.1016/j.cma.2024.117448).
- [32] Z. Lin, Q. Ma, H. Xie, X. Yin, Solving time-fractional partial integro-differential equations using tensor neural network (2025). [doi:10.48550/ARXIV.2504.01440](https://doi.org/10.48550/ARXIV.2504.01440).
- [33] A. A. Kilbas, *Theory and applications of fractional differential equations*, no. 204 in North-Holland mathematics studies, Elsevier, Boston, 2006, includes bibliographical references and index.
- [34] B. Jin, *Fractional Differential Equations: An Approach via Fractional Derivatives*, Springer International Publishing, 2021. [doi:10.1007/978-3-030-76043-4](https://doi.org/10.1007/978-3-030-76043-4).
- [35] D. W. Brzezinski, Computation of gauss-jacobi quadrature nodes and weights with arbitrary precision, in: *2018 Federated Conference on Computer Science and Information Systems (FedCSIS)*, 2018, pp. 297–306.
- [36] A. Chernov, C. Schwab, Exponential convergence of gauss-jacobi quadratures for singular integrals over simplices in arbitrary dimension, *SIAM Journal on Numerical Analysis* 50 (3) (2012) 1433–1455. [doi:10.1137/100812574](https://doi.org/10.1137/100812574).
- [37] I. Podlubny, *Fractional differential equations*, no. v. 198 in *Mathematics in science and engineering*, Academic Press, San Diego, 1999.
- [38] S. Wang, S. Sankaran, P. Perdikaris, Respecting causality is all you need for training physics-informed neural networks (Mar. 2022). [arXiv:2203.07404](https://arxiv.org/abs/2203.07404).
- [39] S. Wang, Y. Teng, P. Perdikaris, Understanding and mitigating gradient flow pathologies in physics-informed neural networks, *SIAM Journal on Scientific Computing* 43 (5) (2021) A3055–A3081. [doi:10.1137/20m1318043](https://doi.org/10.1137/20m1318043).